

1 **Active tectonics in the Kvarner region (External Dinarides, Croatia) –**  
2 **an alternative approach based on new focused geological mapping, 3D**  
3 **seismological and shallow seismic imaging data**

4 **Tvrtko Korbar<sup>1\*</sup>, Snježana Markušić<sup>2</sup>, Ozren Hasan<sup>1</sup>, Ladislav Fuček<sup>1</sup>, Dea Brunović<sup>1</sup>, Nikola**  
5 **Belić<sup>1</sup>, Damir Palenik<sup>1</sup>, Vanja Kastelic<sup>3</sup>**

6 <sup>1</sup> Croatian Geological Survey, Sachsova 2, 10000 Zagreb, Croatia

7 <sup>2</sup> University of Zagreb, Faculty of Science, Zagreb, Croatia

8 <sup>3</sup> Istituto Nazionale di Geofisica e Vulcanologia – INGV, L’Aquila, Italy

9

10 \* Correspondence: [tkorbar@hgi-cgs.hr](mailto:tkorbar@hgi-cgs.hr)

11 **Keywords:** Adriatic microplate, External Dinarides fold-and-thrust belt, earthquakes, active tectonics,  
12 geological mapping, Quaternary sediments.

13 **Abstract**

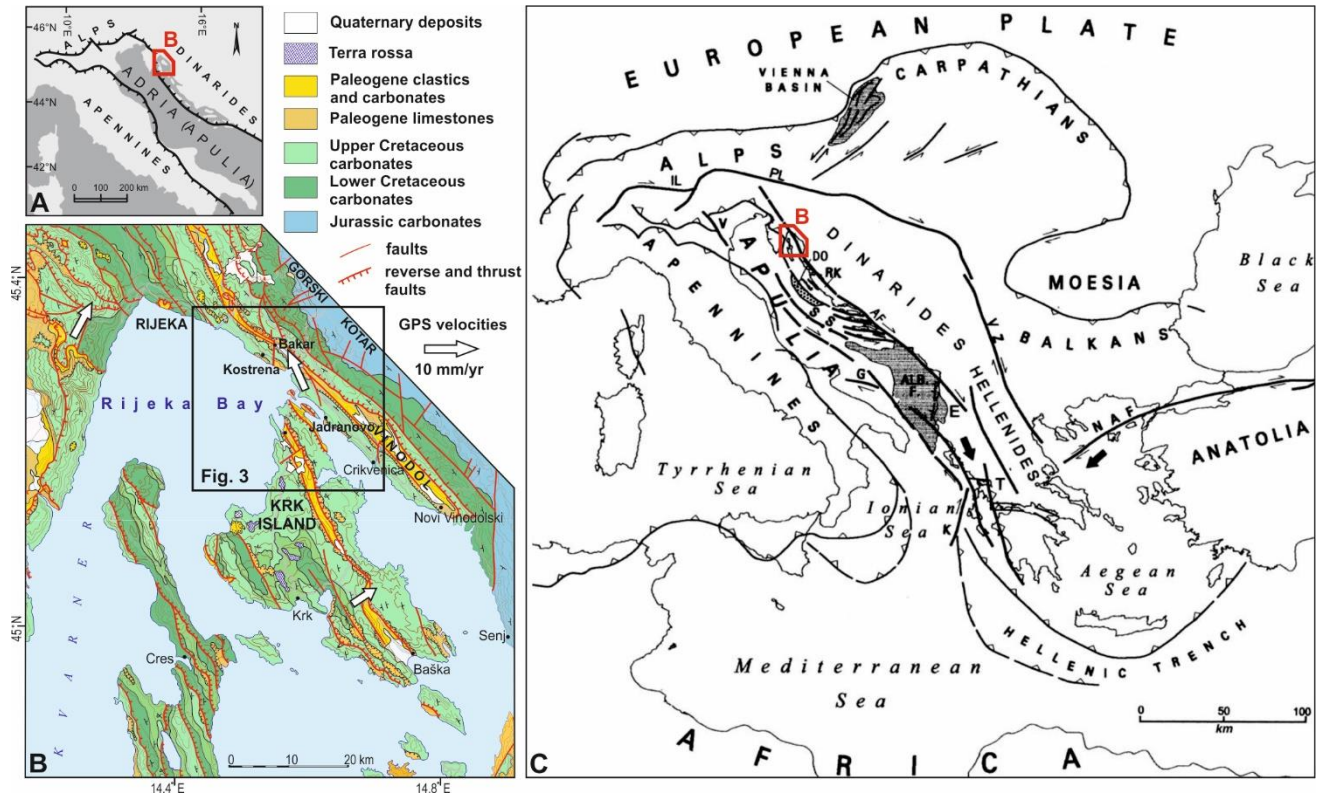
14 Active tectonics in long-lived orogenic belts usually manifests on the pre-existing inherited structures.  
15 In the Kvarner region of the External Dinarides, an area with low-to-moderate seismicity related to the  
16 Adriatic microplate (Adria) northward movement, we deal with faults in predominantly carbonate  
17 rocks within tectonically complex fold-and-thrust belt, which makes the identification and  
18 parametrization of the active structures challenging. Moreover, anthropogenic modifications greatly  
19 complicate access to the surface geological and geomorphological data. This paper demonstrates  
20 results of focused multidisciplinary research, from surface geological mapping and offshore shallow  
21 seismic surveys to earthquake focal mechanisms, as an active fault identification and parametrization  
22 kit, with a final goal to produce an across-methodological integrated model of the identified features  
23 in future. Reverse, normal, and strike-slip orogen-parallel (longitudinal) to transverse faults were  
24 identified during geological mapping, but there is no clear evidence of their mutual relations and  
25 possible recent activity. The focal mechanisms calculated from the instrumental record include weak  
26 to moderate earthquakes, and show solutions for all faulting-types in the upper crust, compatible with  
27 the NE-SW oriented principal stress direction, with the stronger events favoring reverse and strike-slip  
28 faulting. The 3D spatial and temporal distribution of recent earthquake hypocenters indicate their  
29 clustering along predominantly subvertical transversal and steeply NE dipping longitudinal planes.  
30 High-resolution shallow seismic geo-acoustical survey (sub-bottom profiler) of the Quaternary  
31 sediments in the Rijeka Bay revealed local tectonic deformations of the stratified Late Pleistocene  
32 deposits that, along with overlaying mass-transport deposits, could imply pre-historical strong  
33 earthquake effects. Neotectonic faults onshore are tentatively recognized as highly fractured zones  
34 characterized by enhanced weathering, but there is no evidence for its recent activity. Thus, it seems  
35 that the active faults are blind and situated below the thin-skinned and highly deformed early-orogenic  
36 tectonic cover of the Adria. A strain accumulating deeper in the crust is probably irregularly  
37 redistributed near the surface along the pre-existing fault network formed during the earlier phases of  
38 the Dinaric orogenesis. The results indicate a need for further multidisciplinary research that will  
39 contribute to a better seismic hazard assessment in the densely-populated region that is also covered  
40 by strategic infrastructure.

41

42 **Introduction**

43 Kvarner region (Croatia) is situated in the NW part of the External Dinarides (Figure 1A), and is built  
 44 of deformed, uplifted and eroded Mesozoic to Cenozoic predominantly carbonate rocks (Figure 1B).  
 45 The rocks represent detached and backthrust pre-orogenic upper sedimentary cover of the northeast  
 46 moving Adria (Apulia is a synonym, Figure 1C) during the main phase of the Alpine orogenesis in the  
 47 region (Schmid et al., 2008), when a tectonically complex NW-SE striking (so-called Dinaric strike)  
 48 fold-and-thrust belt has been formed in the area (Tari, 2002; Korbar, 2009).

49



50 **Figure 1.** A) A sketch-map of the orogenic fronts in the Adriatic region and the position of the Kvarner region (red  
 51 frame). B) Overview geological map of the Kvarner region (modified after HGI, 2009) and the position of the  
 52 investigated area Bakar-Krk (small frame). C) Overview tectonic map showing major tectonic lineaments in central-  
 53 southern Europe (from Picha, 2002). Note a regionally significant NE Adriatic Fault zone (AF) that crosses the study area  
 54 (see Korbar, 2009 for details).

55 In the Rijeka Bay and the surrounding marine channels (Figure 1A), the submerged karst landscape is  
 56 covered with Quaternary sediments (Juračić et al., 1998). The combined influence of multiple factors  
 57 such as tectonic movements, sea level changes, climate and lithology led to the complex geological  
 58 and geomorphological evolution of the Rijeka Bay (Benac and Juračić, 1998; Benac et al., 2004).  
 59 Erosional and accumulation processes, as well as karstification depth, changed substantially with these  
 60 factors (Benac and Juračić, 1998). The formation of the present-day submerged karst landscape  
 61 occurred due to the post-Last Glacial Maximum (LGM) sea level rise (Correggiari et al., 1996;  
 62 Lambeck et al., 2011; Benjamin et al., 2017). Juračić et al. (1998) estimated that the thickness of the  
 63 Holocene marine sediments in the area is between 2 and 10 m. The greater thickness was determined  
 64 near the mouths of permanent and ephemeral rivers and streams (Juračić et al., 1998). It is likely that

65 there was no connection between the Rijeka Bay and the open Adriatic during glacial periods which  
66 enabled the development of different depositional environments, like karst lakes (Benac & Juračić,  
67 1998; Juračić et al., 1999). However, no systematic sub-bottom studies of the Quaternary sediment  
68 cover have been conducted in this area so far, especially in the context of paleoseismology.

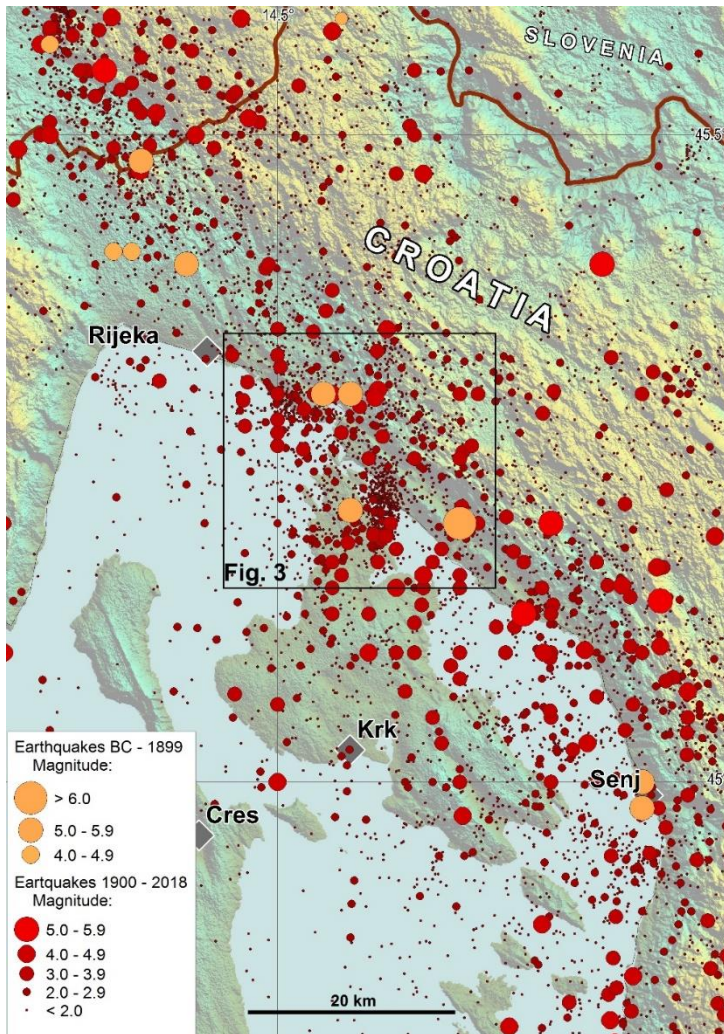
69 The differentially submerged tidal notches in the investigated area (Benac et al., 2004; 2008) are  
70 interpreted as a result of different tectonic subsidence related to the supposed major active thrust in the  
71 Bakar-Vinodol zone (Stiros and Moschas, 2012). However, the differential position of the tidal notches  
72 in the Bakar Bay may be related to another type of local active tectonic movements or could be of a  
73 non-tectonic origin. Nevertheless, recent tectonic activity is indicated also according to the analyses of  
74 the submerged speleothems from the central coastal part of the island of Krk (Surić et al., 2005), and  
75 the results indicate a very slow tectonic uplift of the island, although a subsidence is expected for the  
76 NE Adriatic islands (Surić et al., 2014).

77 The active tectonics in the Adriatic region is related to the motion of the Adriatic microplate (Adria or  
78 Apulia) and the interaction of the microplate with the surrounding Alpine orogenic belts: the Apennines  
79 on the southwest, the Southern Alps on the northwest, and the Dinarides on the northeast (Anderson  
80 and Jackson, 1987; Figures 1A and C). The active deformation in the orogenic belts is probably driven  
81 by the independent motion of the Adriatic plate rather than by the Africa-Eurasia convergence (Oldow  
82 et al., 2002). Under the External Dinarides the Moho depth passes from 40-42 km in its NW to 45 km  
83 in the central and SE sector with local peaks of 50 km (Stipčević et al., 2020). The Adriatic lithosphere  
84 is found deeper below the SE Dinarides and shallower in the NW Dinarides (Šumanovac et al., 2017),  
85 and the Adria migrates generally to the north in respect to Europe while rotating counter-clockwise  
86 around its pole in North Italy (Battaglia et al., 2004; Nocquet and Calais, 2004). Accordingly, the  
87 relative movements of Adria generally increase from the northwest to the southeast and its relative N  
88 to NE displacement in the wider Kvarner region is just a few mm/yr (Weber et al., 2010). However,  
89 the movement directions at the observed points from the investigated area varies between NW and NE  
90 (Altiner et al., 2006; Figure 1B), and it seems that the local active tectonic setting is not as simple as  
91 considered previously (Prelogović et al., 1995; Kuk et al., 2000; Placer et al., 2010). Thus, the Kvarner  
92 region is seismically moderately active, and the earthquakes occur in the upper crust probably along  
93 the tectonic contact of two major crustal segments of the Adria – Adriatic and Dinaridic (Korbar, 2009)  
94 i.e., along the NE Adriatic Fault zone (Picha, 2002; AF on Figure 1C).

95 According to the Croatian Earthquake Catalogue (CEC2018), firstly described by Herak et al., 1996),  
96 the wider Rijeka area exhibits moderate to strong seismicity (Figure 2). Seismic activity here is known  
97 for frequent occurrences of relatively weak earthquakes ( $M < 4.0$ ) and occasional occurrences of  
98 moderate or large ones (Ivančić et al., 2006, 2018). The earthquake hypocenters lie mostly at depths of  
99 up to 20 km, within the seismogenic tectonic zone striking in the NW-SE direction along the coastline.  
100 The Ilirska Bistrica-Rijeka-Vinodol-Senj zone is interpreted as obliquely reverse fault system that  
101 accommodates an oblique subduction of the Adriatic microplate and the compression in the Dinarides  
102 (Kuk et al., 2000; Palenik et al., 2019), along the NE Adriatic Fault zone.

103 The regional seismic data are available in the earthquake catalogue CEC2018. It contains basic  
104 information on more than 110.000 earthquakes that occurred in the period 373BC–2018 in Croatia and  
105 the neighboring areas. The latest version of the catalogue is kept in the archives of the Department of  
106 Geophysics, Faculty of Science, University of Zagreb. Figure 2 shows an overview map of the  
107 epicenters of all earthquakes that occurred in the wider Kvarner (Rijeka) area by the end of 2018  
108 according to the CEC2018. In addition to the recent seismic activity (the period after 1900, since the  
109 instrumental earthquake data exist), also the historical seismicity, which includes earthquakes that

110 occurred in the period before 1900, and whose parameters were determined on the basis of reliable  
 111 macro-seismic data, is displayed. For the historical earthquakes, before 1900, the magnitude was  
 112 derived using macro-seismic data (earthquake intensity).  
 113



114 **Figure 2.** Spatial distribution of earthquakes in the Rijeka epicentral area (Kvarner region, W Croatia and SE Slovenia)  
 115 (373BC – 2018, according to the Croatian Earthquake Catalog - CEC, updated version first described in Herak et al., 1996).  
 116 All the events are from shallow crustal depths (down to 25 km). Red dots are instrumentally recorded events while orange  
 117 dots are historical events. The Rijeka epicentral area has population of ~350,000.  
 118  
 119

120 The most significant earthquakes (with intensities greater or equal to VII °MSK) occurred in 1323,  
 121 1750, 1776, 1838, 1870, 1904 and 1916. The strongest historical local earthquake occurred in 1323  
 122 with intensity at the epicentre  $I_0 = IX$  °MSK and estimated magnitude of 6.7. After that earthquake,  
 123 there were no more significant recorded events on the Ilirska Bistrica–Vinodol fault zone until 1750  
 124 when a large earthquake series occurred in the hinterlands of the town of Bakar. The strongest event  
 125 in this series happened in 1750. Until October 1754 up to 3000 earthquakes and rumbles were felt or  
 126 heard in that area (*Acta Buccarana*, Gratianus, 1755; Herak et al., 2017; Kišpatić, 1891; Laszowski,  
 127 1923; Radics, 1903; Tomsich, 1886). Therefore, macroseismic intensity has been estimated as a  
 128 cumulative value for all the earthquakes from that series which could have caused damage to the  
 129 buildings. The main event caused a lot of damage in Rijeka in a way that many people had to live in  
 130 huts built at the seashore. The maximum intensity of the event is evaluated as VIII °MSK scale  
 131 (estimated magnitude is  $M = 5.7$ ). According to the recent data analysis for this event (Herak et al.,

132 2017) the epicentre was located again near Bakar. Very strong earthquake occurred in 1776, and  
133 according to the historical data (Perrey, 1850) it was found that the event was most strongly felt in  
134 Bakar, but it was also felt in Rijeka and Trieste. Assigned intensity at the epicentre was VII °MSK.  
135 According to available records, in the epicentral area of the Krk Island the strongest earthquake  
136 occurred in 1838. Maximum intensity was VII °MSK, felt on the northern part of Krk island and around  
137 Bakar Bay. That is why the Bakar-Krk area is in focus of our research. A destructive earthquake  
138 occurred in 1870 near Klana (10 km NW of Rijeka), with the intensity at the epicentre VIII °MSK.  
139 This is one of the most important earthquakes that happened in the vicinity of Rijeka and is very  
140 important for the seismic hazard of wider Rijeka area. Moderately strong earthquake occurred near  
141 Bakar in 1904. Macroseismic intensity in the epicentre was estimated VII °MSK. A very strong  
142 earthquake occurred in 1916, about ten kilometres to the east from Novi Vinodolski (intensity at the  
143 epicentre was VIII °MSK). The seismograph in Zagreb recorded the event; therefore, it was possible  
144 to calculate its magnitude as 5.8.

145 The existing seismotectonic model of the Kvarner region is based on 2D analysis of the hypocenters  
146 used for a traditional interpretation of NE-dipping reverse seismogenic faults formed because of  
147 displacements of the Adriatic microplate segments under the Dinarides (Prelogović et al., 1995; Kuk  
148 et al., 2000). However, one of the regional geological models highlights structural complexity in the  
149 crustal scale derived from a multi-phase tectonics that characterizes this part of the orogenic belt  
150 (Korbar, 2009). The seismicity in the Kvarner (Rijeka) region is probably a consequence of the escape  
151 tectonics (Picha, 2002) along relatively steep crustal fault zone striking in Dinaric direction (NW-SE)  
152 that is recognized regionally as the NE Adriatic Fault zone (AF on Figure 1C). Possible active faults  
153 that belong to a wide zone of the AF are recognized during the more focused studies in this part of  
154 External Dinarides (Cunningham et al., 2007; Moulin et al., 2016; Žibret and Vrabec, 2016). Thus,  
155 there is an open question of a SE continuation of the recognized active faults on the surface in the  
156 Rijeka epicentral area (Figure 2). Besides, there is an open question of a possible active tectonic role  
157 of other inferred faults e.g., reactivated early-orogenic detachments and transversal faults to the main  
158 strike of the Dinarides. The former has been recognized on the interpreted regional geological cross-  
159 section across the Velebit Mountains, while the later are generally recognized in the investigated area  
160 as the Kvarner fault zone (Korbar, 2009 and references therein).

161 There are many limitations to the research on geological structures in the area. The deep seismic  
162 profiles are available only for the Rijeka Bay. However, the images are of low quality and are especially  
163 chaotic in the investigated marginal parts of the Bay. Besides, there are no boreholes in the investigated  
164 area that could allow a correlation of the low-quality seismic data. That is why the data were not useful  
165 neither in the previous seismotectonical studies in the area (Prelogović et al., 1995; Kuk et al., 2000)  
166 nor in our research.

167 Three composite seismogenic sources were proposed for the Rijeka Bay and Krk island, all  
168 characterized by the Dinaric strike (Kastelic and Carafa, 2012; Kastelic et al., 2013). The more internal  
169 sources run along the shore of the mainland in Rijeka area (the northern margin of the Bay) towards  
170 SE, while the more external source occupies areas of Krk island. The first two sources have mid-to-  
171 steep NE dipping angles with reverse-right lateral kinematics, while the third source has mid NE  
172 dipping angle with a less pronounced oblique right lateral kinematic component. The compilation of  
173 these sources are mainly based on different geologic and morphologic data integrated with  
174 seismotectonic cross-sections of the existing seismotectonic models (Kuk et al., 2000) and on the  
175 earthquake data. All sources are located in the upper crust with maximum depth of 18 km. It has been  
176 recognized that across the region more internal faults have become steeper dipping in the course of

177 evolution of the External Dinarides, and are therefore considered long-lived features with a weaker  
178 rheology (Kastelic and Carafa, 2012).

179 Concerning the seismic hazard in the region that is characterized by more than 350.000 inhabitants and  
180 the strategic infrastructure, the latest project was "The Harmonization of Seismic Hazard Maps in the  
181 Western Balkan Countries Project" (BSHAP), that was financed by NATO-Science for Peace Program.  
182 One of the main outputs of the project was the new probabilistic seismic hazard maps for Western  
183 Balkans (Güllerce et al., 2017). These maps were obtained by implementation of the smoothed-gridded  
184 seismicity approach. The results are expressed in terms of peak horizontal acceleration (PGA) for 95  
185 and 475 years return periods aligned with Eurocode 8 requirements, for the soil type A. Based on these  
186 results it can be seen that in this work investigated area is characterized with PGA in the intervals 0.06-  
187 0.08 g (for return period 95 years - probability of exceedance 10% in 10 years) and 0.16-0.20 g (for  
188 return period 475 years – probability of exceedance 10% in 50 years).

189 In this paper we deal with faults in predominantly carbonate (karst) terrains built of highly deformed  
190 and fractured rocks within tectonically complex fold-and-thrust belt, characterized by little Quaternary  
191 deposits on the highly dissected karst terrain, which makes the identification and parametrization of  
192 the active structures challenging. The region is also densely populated and anthropogenic modifications  
193 greatly complicate access to the surface geological and geomorphological data. That is why the key  
194 evidence of the active tectonics in the deep subsurface are earthquake hypocenters. The indications of  
195 the active faults at the surface we tried to find in new focused geological mapping and structural  
196 research, as well as in the shallow seismic imaging of the Quaternary sediments that cover the  
197 predominantly carbonate bedrock in the Rijeka Bay, and in the surrounding channels and bays. We  
198 focused to the surroundings of the small town of Bakar and the northern part of the Krk Island, so-  
199 called Bakar-Krk area (Figures 1 and 3) that is characterized by rare strong historical earthquakes,  
200 weak to moderate clustered events (tremors), relatively well-known surface geology and the recognized  
201 Quaternary sub-bottom sediment deformations.

202 This paper presents a multidisciplinary approach to definition of possible seismogenic faults that  
203 include classical geological and structural research on the surface, shallow seismic survey in marine  
204 area, and the focused 3D analyses of the selected hypocenters. The 3D modelling of the active faults  
205 is here for the first time applied in the area of External Dinarides, following the methodology developed  
206 on the 22 March 2020 Zagreb earthquake sequence (Markušić et al., 2020). Combination of the results  
207 from the various methods allow us to narrow in on structures that could be active.

208

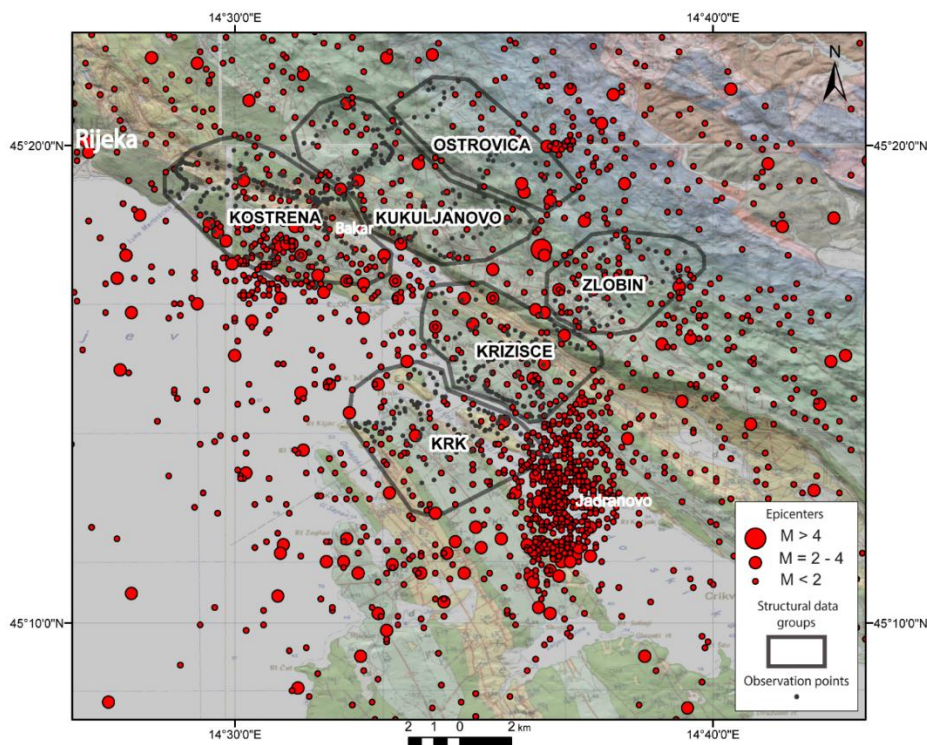
## 209 **Data and Methods**

### 210 *Geological mapping and structural analysis*

211 For the purpose of interpretation of the near surface geological structure, we mapped a few kilometers  
212 wide zones across the investigated area Bakar-Krk (Figure 3). The mapping was based on the  
213 lithostratigraphical units defined during previous mapping of the neighboring islands (Fuček et al.,  
214 2015; Palenik et al., 2019). The objective of the geological mapping was a lithostratigraphic  
215 harmonization of the existing Basic geological maps of the area in scale 1:100.000 that are based on  
216 chronostratigraphy and are not geologically harmonized in between the sheets (Šikić et al., 1969; 1972;  
217 Šušnjar et al., 1970, Savić and Dozet, 1985). The new map is used for the interpretation of two  
218 representative geological cross-sections approximately transversal to the main strike of the Dinaric  
219 structures (Figures 4 and 5).

220 Structural-geological investigations of the area (Figure 3) were conducted simultaneously with the  
 221 geological mapping. For the purpose of geological mapping an attention was given also to the detection  
 222 of potentially active surface faults that are presumably marked by specific geomorphological features.  
 223 The features were recognized on aerial orthophotographs using the public web map service  
 224 (<https://geoportal.dgu.hr/>). The structural data are obtained by field measurements and include dip  
 225 direction and dip angle of fault planes, orientation of carbonate slickensides defined by azimuth and  
 226 plunge, and the sense of movement. The data are used for kinematic analyzes and determination of  
 227 fault kinematics in relation to the past stress fields.

228 During geological mapping and simultaneous structural field investigations 315 fault plane data  
 229 (Supplement Tables) with all parameters required for kinematic analysis in the whole study area have  
 230 been collected. The structural data are spatially grouped in six groups (areas) according to the position  
 231 within the recognized general geological structures (Figures 3 and 6). Based on kinematic criteria and  
 232 sense of movements, the structural data were separated into main groups of faults and processed by  
 233 Tectonics FP software (Ortner et al., 2002). Using the P–T axis method (Marrett and Allmendinger,  
 234 1990) theoretical maximum ( $\sigma_1$ ), intermediate ( $\sigma_2$ ) and minimum stress axes ( $\sigma_3$ ) were calculated,  
 235 whereas using the Right Dihedra Method (Angelier and Mechler, 1977) paleo-synthetic focal  
 236 mechanisms as representations of the paleo-stress fields for the analyzed faults were determined.



237

238 **Figure 3.** The investigated Bakar-Krk epicentral area. Red dots mark the most relevant instrumentally recorded  
 239 earthquakes in period 1979 to 2018 ( $M$  0-3.6 and only one event  $M$  4.5), showing the two recognized earthquake clusters  
 240 in the areas of Kostrena and Jadranovo. Gray dots mark observation points in the area of the focused geological fieldwork  
 241 while the 6 labeled irregular polygons mark spatial groups of structural data (see Results and Figure 6). The transparent  
 242 geological map in the background is from the Basic geological maps of the area (Šikić et al., 1969; 1972; Šušnjar et al.,  
 243 1970, Savić and Dozet, 1985), that is underlain by a semi-transparent hillshade map.

244

## 245 *Seismological analysis and 3D modelling of the active faults*

246 A fault plane solution (FPS), also called focal-mechanism solution, is a simple way of studying the  
247 earthquake faulting process. Its goal is to determine the geometry and sense of motion on the fault. In  
248 this work we analysed the spatial distribution of the first P-wave motion polarities to obtain fault-plane  
249 solutions for earthquakes recorded in the investigated area by the Croatian seismic network. The FPS  
250 from previous studies in the area (Markušić et al., 2019) and from earthquakes in Croatian source  
251 mechanism database (Archive of the Department of Geophysics) were updated with FPS calculated  
252 within this research for the study area and magnitudes  $M \geq 2.7$  (Figure 7). It should be noted that all  
253 events are weak to moderate earthquakes ( $M 2.7 - 4.5$ ).

254  
255 A 3D analysis of the seismic activity in the considered area was based on temporal and spatial  
256 distribution of the selected recent earthquakes (Figure 3). With the aim to analyze the most relevant  
257 seismological data (especially concerning the focal depth), only the instrumentally recorded  
258 earthquakes from the catalog from 1979 to 2018 were selected. Near-surface probably non-tectonic  
259 events and the events automatically calculated to virtual infinity depth were eliminated. Because of too  
260 large number of the hypocenters (Supplement 1), we focused on two biggest earthquake clusters  
261 located east of the island of Krk (“Jadransko” cluster), and west of Bakar (“Kostrena” cluster) (Figure  
262 3), as well as to the coastal zone of the Dinaric strike along the Bakar-Vinodol flysch zone (Figure 1)  
263 that is interpreted previously as a major active thrust of the External Dinarides (Stiros and Moschas,  
264 2012). Thus, the analysis is based on the hypocenters of the events that are relatively well located,  
265 considering the development of the quality and increasing number of the instruments.

266 Seismological data provided the input for preliminary active faults modelling. The input data comprise  
267 recorded hypocenters including magnitude value, coordinates, depth, and the precise time of each  
268 shock for the earthquake sequences in the time span from 1979 to 2018 (Figure 3; Supplement 1). Most  
269 of the hypocenters dated from 2001 – 2017, due to gradual densification of the seismological grid in  
270 the wider area, while older data mostly represent significant seismic events holding relatively high  
271 magnitude values. The data was processed and represented spatially and temporally, including a time-  
272 lapse visualization using ESRI ArcSceneTM 10.2.1. Geological interpretation of the processed data  
273 included both spatial and temporal 3D visual analysis of the hypocenters. The methodology for  
274 extraction of hypocenters was based on visual extraction of hypocenters concentrated around a  
275 suggested specific fault plane. A total of 943 events were used for visual analysis and extraction of  
276 three datasets used for interpretation of the fault planes/zones. Selected datasets were used as input for  
277 the structural modelling of fault planes (Figure 8) performing the inverse distance weight (IDW) point  
278 interpolation method, using Move 2019.1 (cf. Markušić et al., 2020).

279

## 280 *High-resolution shallow seismic survey*

281 In order to detect possible (sub)recent faults or other evidence of tectonic activity in the marine  
282 environment, we conducted a high-resolution seismic reflection survey using an Innomar SES-2000  
283 light. We chose the SES-2000 light as the most suitable, as it is a parametric sub-bottom profiler (SBP)  
284 designed for application at water depths down to 400 m, with sediment penetration up to 50 m (Winton,  
285 2020; Wunderlich and Müller, 2003) and theoretical resolution of 5 to 10 cm (Daxer et al., 2019; Wang  
286 et al., 2019). It uses a high frequency for echo sounder and bottom track, and low frequency for sub-  
287 bottom data. Together with high ping rate (up to 40 pings per second) it allows a good penetration and  
288 high resolution of collected data. Further technical information and advantages of this system in similar



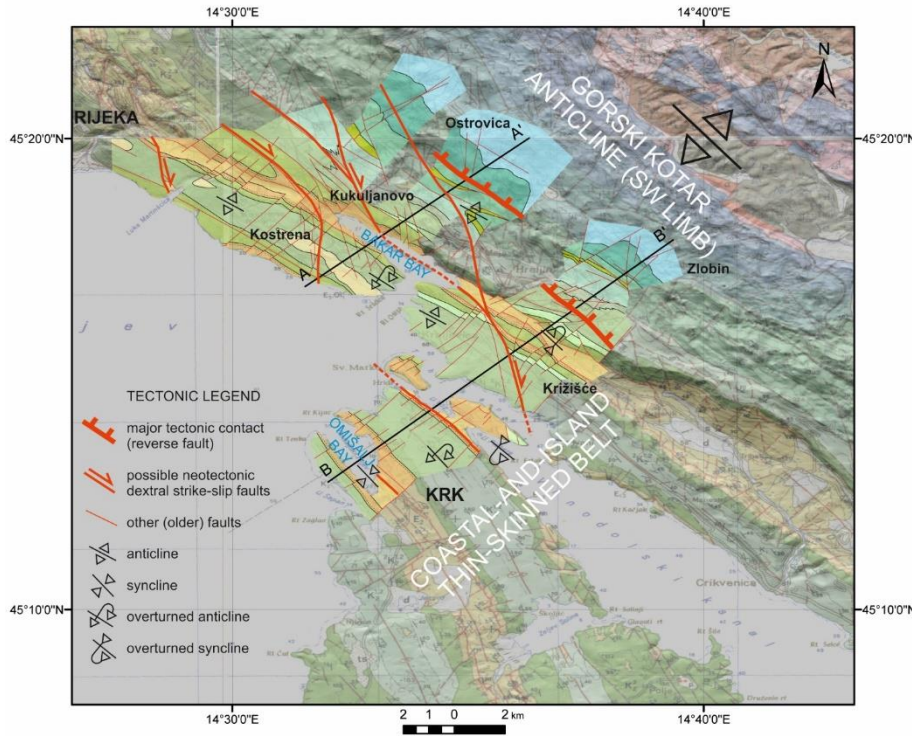
289 environments can be found in Unnithan and Rossi (2018), Yutsis et al. (2014), Missiaen (2008) and  
290 Wunderlich (2007). During the survey, we used low frequency of 6 or 8 kHz and high frequency of 12  
291 kHz. A SBP was side-mounted on a 6 m long shallow draught vessel with low noise engine. For  
292 positioning and vessel motion corrections, we used Applanix POS MV WaveMaster combined with  
293 two Trimble GNSS antennas and RTK unit to receive corrections from CROPOS network (Croatian  
294 Positioning System). During the survey, the vessel speed was maintained at 3.5 knots. Processing and  
295 interpretation of seismic data was made in GeoSuite Allworks software. We acquired 65 acoustic  
296 profiles with total length of 264 km (Figures 9 and 10).

297

## 298 **Results**

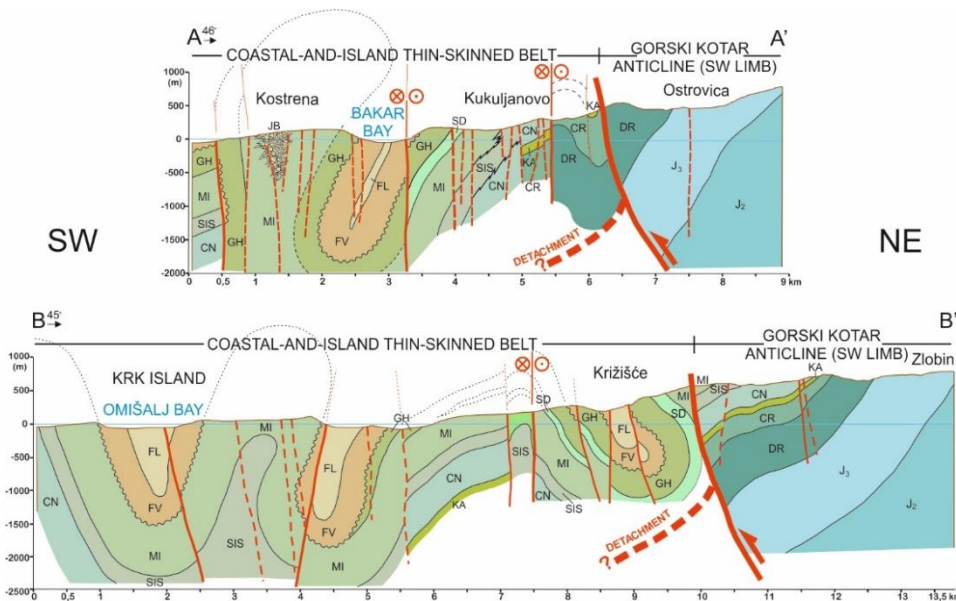
### 299 *Geological cross-sections and structural analysis*

300 Two geological cross sections are constructed along the mapped zones (Figures 4 and 5). Both cross-  
301 sections highlight the complexity of the near surface geological structure in the investigated area. There  
302 are two main large-scale uppermost crustal geological structures: the strongly deformed coastal-and-  
303 island belt on the SW, and the SW limb of the huge Gorski kotar anticline on the NE. The coastal-and-  
304 island belt is characterized by tightly folded, faulted and strongly fractured predominantly middle  
305 Cretaceous to Paleogene carbonates and some Paleogene clastic rocks (predominantly flysch). Such a  
306 structure is probably superimposed on the major detachment (master thrust fault) formed at  
307 rheologically weak horizon within the Lower Cretaceous succession during the Eocene thin-skin  
308 tectonic phase of the orogenic evolution of the External Dinarides (Korbar, 2009). The SW dipping  
309 south-western limb of the huge Gorski kotar anticline is built of the relatively tectonically intact (well  
310 preserved) Jurassic to Lower Cretaceous carbonate rocks that further to the NE disconformably overlay  
311 Paleozoic to Triassic core of the anticline (Herak, 1980; Savić and Dozet, 1985). The contact of the  
312 huge Gorski kotar anticline and the tightly folded coastal-and-island belt could be the major Oligocene  
313 thick-skin fault that dissected the primary thin-skin detachments (Korbar, 2009) although the  
314 detachment could be formed simultaneously with the formation of Gorski kotar anticline along the  
315 major reverse fault (Figure 5).



316

317 **Figure 4** Simplified new geological map of the area of focused fieldwork (full color overlay). The major fault (the  
 318 thickest red lines) delineate the Gorski kotar anticline and the coastal-and-island thin-skinned belt. Possible neotectonic  
 319 dextral strike-slip faults on the surface are marked by medium thick red lines and arrows. Position of the two  
 320 representative geological cross-sections A-A' and B-B' are indicated (**Figure 5**). The transparent map in the background  
 321 is a compilation of the regional Basic geological maps (Šikić et al., 1969, 1972; Šušnjar et al., 1970; Savić and Dozet, 1985)  
 322 combined with a semi-transparent hillshade.



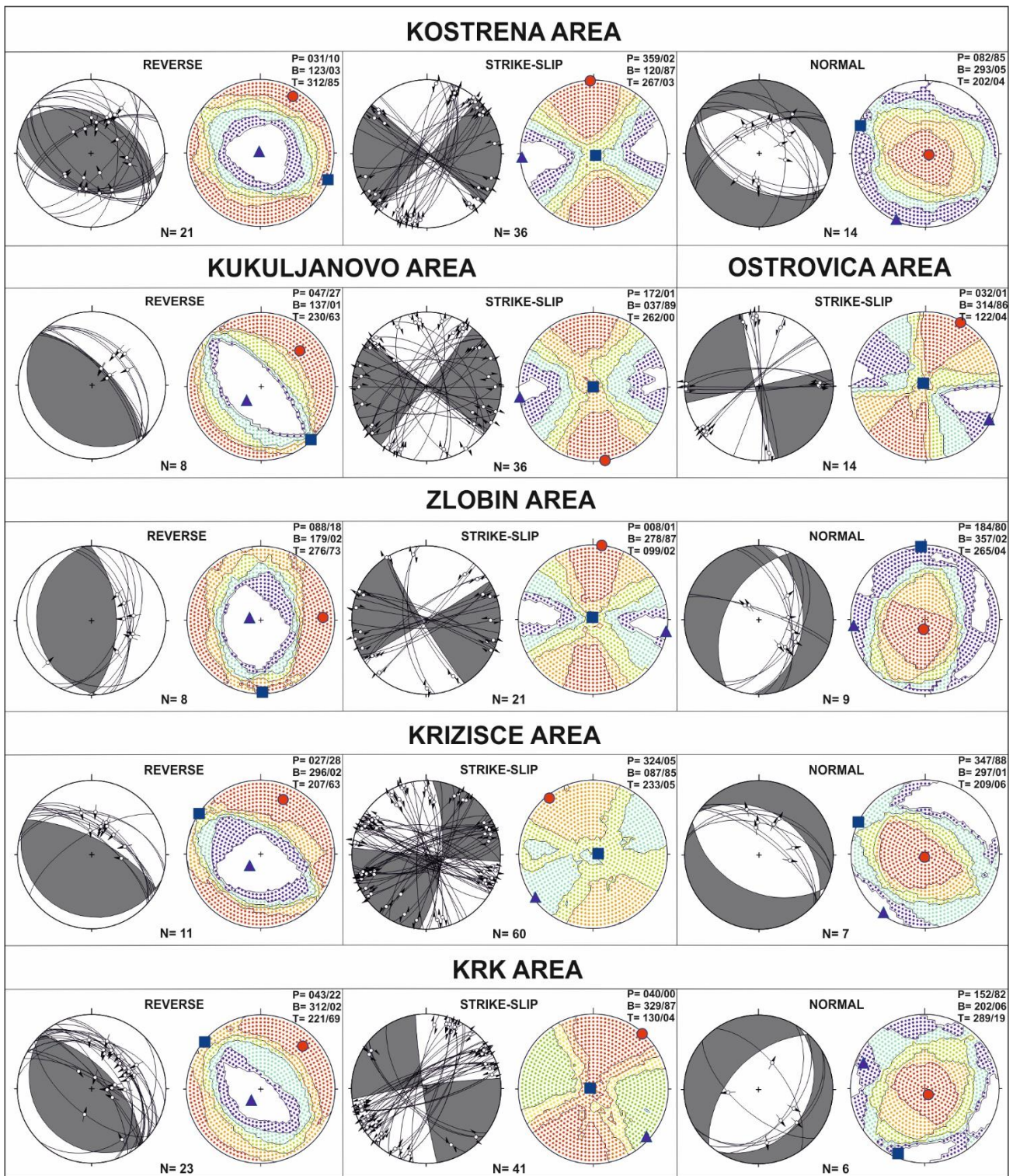
323

324 **Figure 5** Representative transversal geological cross-sections A-A' and B-B' (location map on Figure 4) show tightly  
 325 folded early-orogenic coastal-and-island thin-skinned belt on the SW and the SW limb of the huge Gorski kotar anticline  
 326 on the NE. Major tectonic contact of the two zones, supposed early-orogenic detachment (cf. Korbar, 2009) and possible  
 327 dextral neotectonic strike-slip faults are indicated. Abbreviations of the lithological units are after Fuček et al., 2015).

328 The coastal-and-island belt is built of kilometre-scale asymmetrical, isoclinal and overturned folds with  
329 amplitudes of up to 2 km, that imply a significant amount of horizontal shortening during the early-  
330 orogenic detachment folding (Figure 5; Korbar, 2009). The large NW-SE striking longitudinal  
331 geomorphological carbonate ridges generally mark anticlines. The Paleogene flysch rocks are partly  
332 eroded from the cores of the synclines and thus the synclines form distinct geomorphological valleys  
333 and elongated bays. A system of small NE-SW and NNW-SSE striking transversal faults  
334 insignificantly dissect the fold limbs and were probably formed as conjugated faults during the folding.  
335 The predominantly steep faults strike along the fold axes, and in places dissect the axes along the  
336 NNW-SSE striking fault segments, implying that the steep faults are relatively younger than the folds  
337 itself (Oligocene-Miocene?). Thus, the steep faults have (inverse) sigmoidal appearance on the map,  
338 although there are only a few tens to few hundreds of meters offsets of the geological boundaries of  
339 the mapped units along the faults (Figure 4).

340 The analyses of the geological map and the orthophoto images revealed the selective erosion and  
341 increased weathering of carbonate rocks along the sigmoidal faults that could be a geomorphological  
342 expression of a possible neotectonic activity of the faults. Nevertheless, a braided system of relatively  
343 younger predominantly dextral strike-slip faults is recognized in the area (Figure 4).

344 The observed faults at the scale of individual outcrops in the investigated area are characterized by dip-  
345 slip, strike-slip, and oblique-slip kinematics. In each of the six selected study areas (Figure 3), fault  
346 data were divided into three main categories according to the sense of the movement: reverse, strike-  
347 slip and normal faults (Figure 6).



348

349 **Figure 6.** Structural diagrams for the faults of the investigated area ([Supplement Tables](#)). The red dots, rectangles, and blue  
 350 triangles indicate P, B and T kinematics axis, respectively.

351 Reverse faults on the outcrops in the whole investigated area are characterized by the NW–SE strike,  
 352 dipping both towards the NE and the SW. The exception is the Ostrovica area where reverse faults are  
 353 characterized generally by the N–S strike with dip direction to the E and the W. Reverse faults with  
 354 NE–SW strike direction are relatively rare in the investigated area. Structural analysis of the

355 representative paleostress field for the reverse faults indicates a compression associated with P-axis  
356 dominantly trending NE–SW, whereas the T-axis mostly dipping towards the SW. Some of the  
357 observed reverse fault planes were characterized by structural reactivation, with slickenside indicating  
358 different movements, since the reverse, normal, and horizontal movements are observed on the same  
359 fault planes.

360 Observed strike-slip faults (both dextral and sinistral) in the study area are characterized by steeply  
361 dipping geometry and a variety of strikes. However, there are three predominant strike directions of  
362 the strike-slip faults: NE–SW, N–S and NW–SE, while E–W strike is relatively rare. Kinematic  
363 analysis shows that strike-slip faults of the Kostrena, Kukuljanovo and Zlobin area formed or have  
364 been active in the paleostress field with the N–S trending P-axis. Strike-slip faults of the Ostrovica and  
365 Krk area associated with the NE–SW trending P-axis and the T-axis trending NW–SE, while strike-  
366 slip faults of the Križišće area are characterized by NW–SE trending P-axis and the T-axis trending  
367 NE–SW. Some of mapped strike-slip fault planes were also characterized by structural reactivation,  
368 with slickenside indicating both dextral and sinistral movements.

369 Normal faults in the study area are also characterized by different strike direction. In the Kostrena and  
370 Križišće NW–SE strike predominates. These normal fault planes were formed within the paleostress  
371 field with a subvertical P-axis and the subhorizontal T-axis trending NE–SW, which suggested NE–  
372 SW directed extension. In the Zlobin area, normal fault planes are generally N–S striking and kinematic  
373 analysis indicated that these faults were formed within the paleostress field associated with the  
374 subvertical P-axis orientation 184/80 (dip direction/dip angle) and subhorizontal T-axis trending E–W,  
375 resulting in the E–W extension. In the Krk area strike direction of normal fault planes is mostly NE–  
376 SW and kinematic analysis of this faults shows NW–SE directed extension.

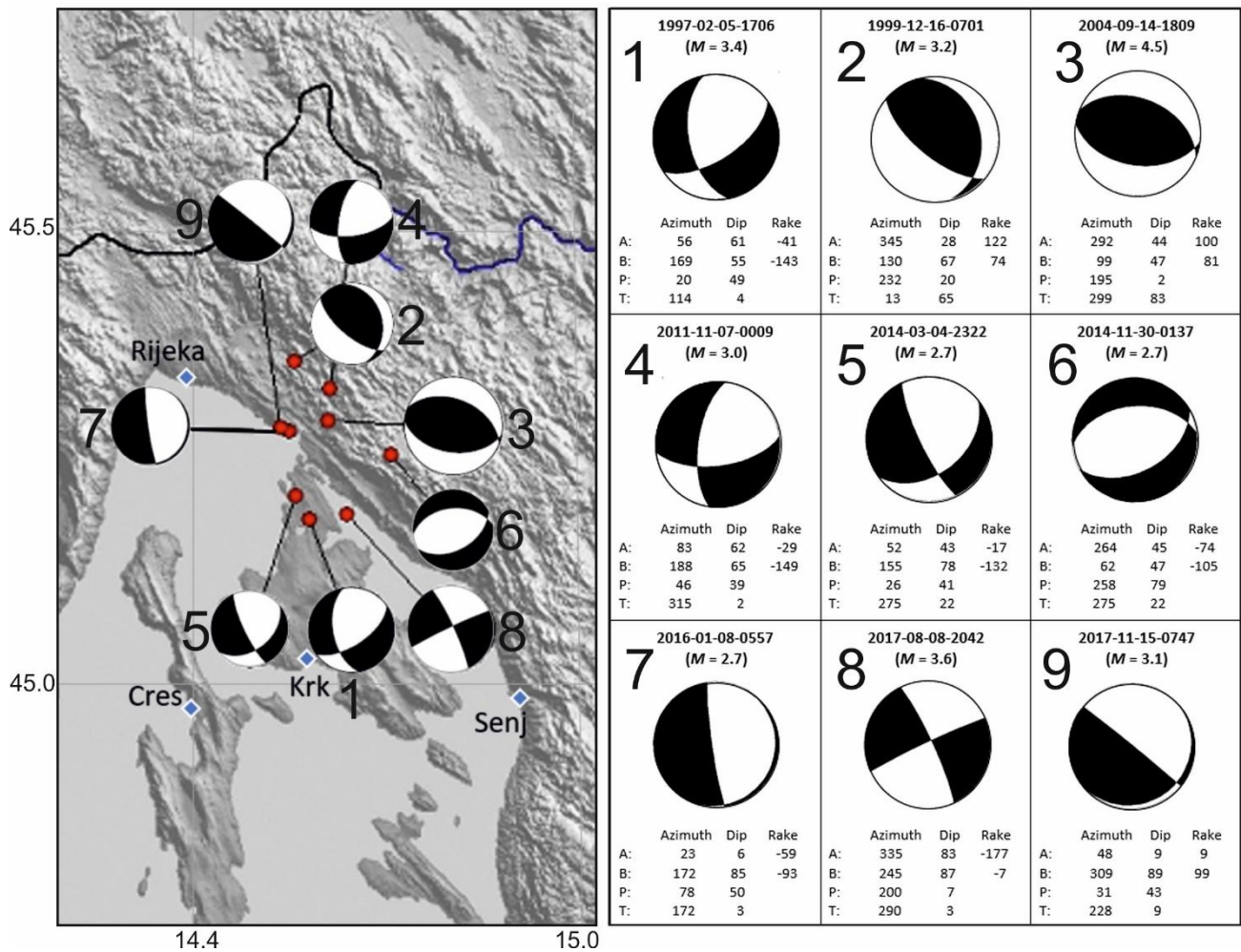
377 Cross-cutting relationships between mapped reverse, strike-slip and normal faults are not sufficiently  
378 determined during field observations, therefore no conclusions can be made about their relative age-  
379 relationship. However, the presented structural data indicate a polyphaser tectonic history of the  
380 investigated area.

381

### 382 *Focal mechanisms of earthquakes in the Bakar-Krk area*

383 The fault plane solutions (FPS) in a relatively small investigated area cover a complete range of  
384 possible earthquake mechanisms (Figure 7). The reverse FPSs are oriented generally parallel to the  
385 Dinaric strike and the eastern Adriatic coast, while the FPSs of normal, oblique and strike-slip faults  
386 indicate activity of a fault system aligned parallel and transversal to the strike. The principal tectonic  
387 stress in the area according to the FPS is generally NE-SSW.

388



389

390 **Figure 7.** Focal mechanisms for the selected earthquakes ( $M \geq 2.7$ ) in the wider Bakar-Krk area and detailed information  
 391 about the nine fault plane solutions (FPS) for the earthquakes (from the Croatian source mechanism database, updated  
 392 version of Marušić et al., 2019). Black areas on the lower focal hemisphere mark compression. Azimuth, Dip, and Rake  
 393 mark the azimuth of the fault strike, fault dip and movement direction along the fault plane. Relation of the FPS with  
 394 possible active structures is shown on Figure 12.

395

### 396 *3D analyses of seismologically constrained fault planes*

397 We tentatively examined the spatial distribution of the instrumentally recorded seismic events in the  
 398 investigated area presuming they all have tectonic origin and that the relatively short period events are  
 399 related through their hosting structure (Figure 8; Supplements 1 and 2). Based on the selected datasets  
 400 (Table 1), three faults were modelled using inverse distance weight (IDW) interpolation of the pre-  
 401 selected datasets (see Data and Methods for explanations).

Fault Name	Abbrev.	Dip azimuth / Dip angle	Number of hypocenters extracted	Time range	Magnitude (M)	Depth (km)

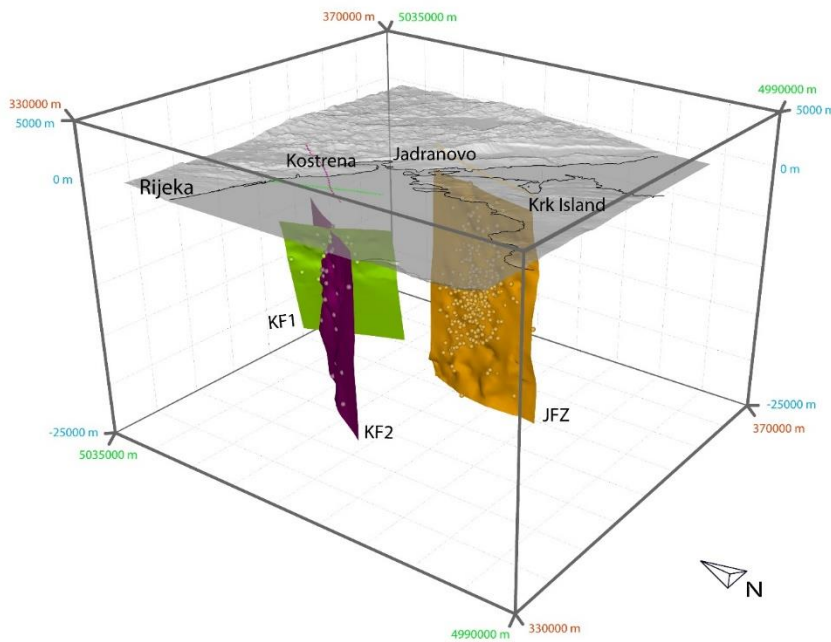
Jadranovo Fault Zone	JFZ	103/89	420	Aug., 8–30, 2017	0–3.6	2.6–19.9
Kostrena Fault 1	KF1	69/64	32	Sept.–Nov. 2017	0–3.1	5.4–10.8
Kostrena Fault 2	KF2	127/89	32	Sept.–Nov. 2017	0–2.1	4.8–21.2

402 **Table 1.** A list of modelled active faults and overview of input data (extracted hypocenters) used for the interpolation of  
 403 the fault plains (the complete data are available on request).

404 The largest dataset was analyzed in the Jadranovo area, where the hypocenters are clustered generally  
 405 along a subvertical broad fault zone striking generally NNE-SSW. Hypocenters are located from a few  
 406 down to 20 kilometers (**Table 1**).

407 In the area of Kostrena, we interpreted two possible faults according to the analysis of the spatial and  
 408 temporal occurrence of the selected earthquake clusters: Kostrena fault 1 (KF1) and Kostrena fault 2  
 409 (KF2). The KF1 has fault plane steeply dipping to the ENE and striking NNW–SSE (generally Dinaric  
 410 strike), and is characterized by the hypocenters located in the middle depths. The KF2 is characterized  
 411 by a subvertical fault plane striking generally NE–SW that is derived from middle to deep seated  
 412 hypocenters.

413 In the area of Bakar Bay and its hinterland we were not able to select any spatially and temporally  
 414 related cluster of hypocenters needed for the interpretation of possible active fault plane.



415 **Figure 8.** 3D model of the selected earthquake hypocenters and the interpreted fault planes in the area of Kostrena and  
 416 Jadranovo (see also **Supplement 2**). Broken lines in the related color mark surface projections of the modelled faults (map  
 417 of the epicenters and the faults is shown on **Figure 12**). Coordinate grid is HTRS96-TM. KF-Kostrena fault (1 and 2). JFZ  
 418 – Jadranovo fault zone.  
 419

420 This preliminary approach of fitting hypocenter locations does not match well with the calculated  
421 focal mechanisms investigated in this paper (Figure 7) neither with other more regional solutions.  
422 Thus, this is an attempt to see how different data fit together. We do not consider it representative at  
423 this stage and further more dedicated and detailed approach in modelling spatial seismicity patterns  
424 in possible active fault structures is needed.

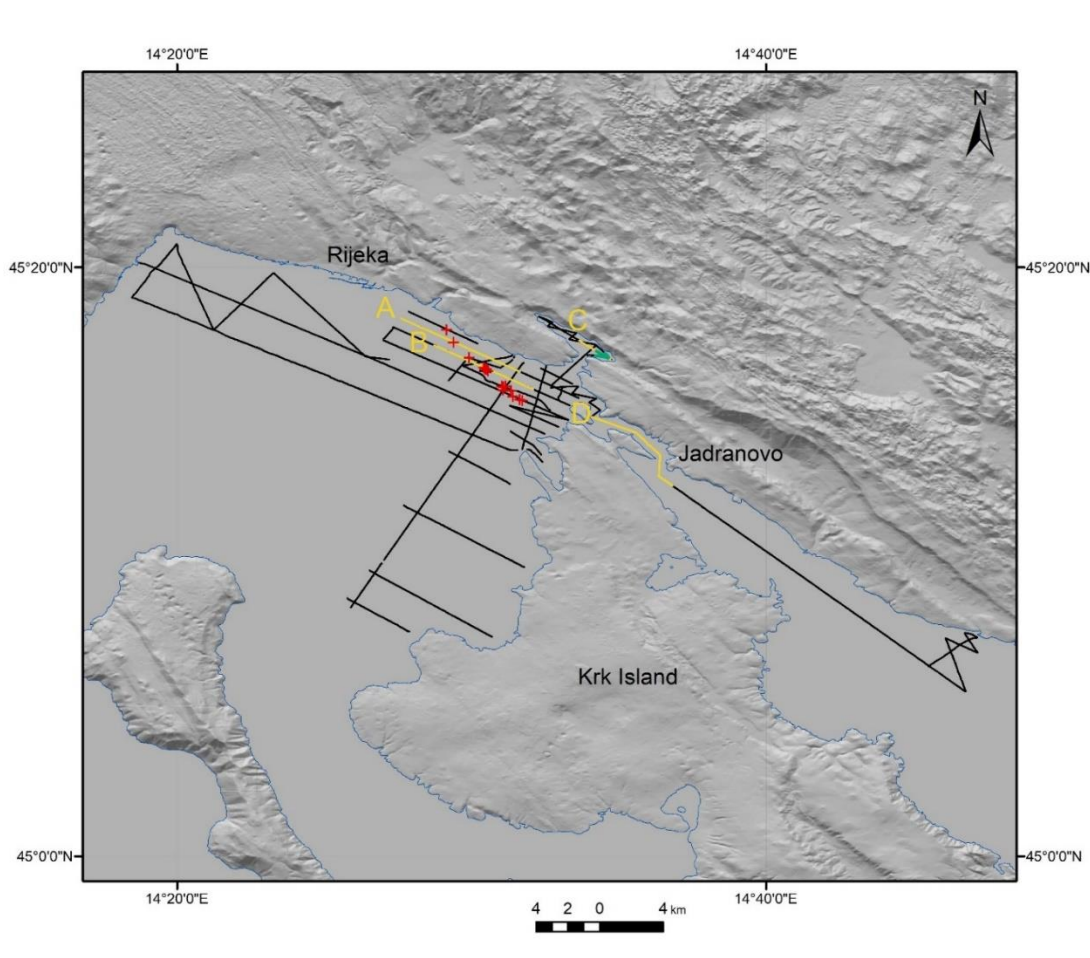
425

### 426 *High-resolution shallow seismic data*

427 The trackline grid (Figure 9) was irregular with line separation from 200 m up to 4.3 km in attempt to  
428 cover a larger area and detect as many tectonic deformation indicators as possible. Twenty-five profiles  
429 were oriented parallel to the coastline, while 12 were perpendicular.

430 Analyses of 264 km of shallow seismic images revealed that the acoustic signal penetration into the  
431 sediment was up to 39 m in Rijeka Bay (with sound velocity estimated at 1500 m/s), with water depth  
432 down to 64 m. The sides of the Rijeka Bay are very steep and rocky, reaching depths of over 50 m  
433 approximately 500 m away from the coast. The rest of the bay has a flat and smooth bottom with  
434 sediment thickness larger than signal penetration. Recent fine-grained sediments (mud) predominantly  
435 cover the Rijeka Bay sea bottom (Juračić et al., 1999). Sediment distribution was influenced by sea  
436 level changes that occurred during the Late Pleistocene (Benac & Juračić, 1998). As a consequence of  
437 fine-grained sediments, it was possible to achieve a good acoustic signal penetration in the Rijeka Bay.  
438 Penetration of the acoustic signal in the Mala Vrata and Vinodol Channel was up to 20 m but  
439 dominantly 5 m or less, due to the seabed consisting of gravel and sandy mud (Juračić et al., 1999), but  
440 also due to shallow depth to carbonate bedrock. Acoustic signal penetration in significantly shallower  
441 Bakar Bay (down to depth -38 m) is up to 20.5 m when it reaches acoustically impermeable bedrock.

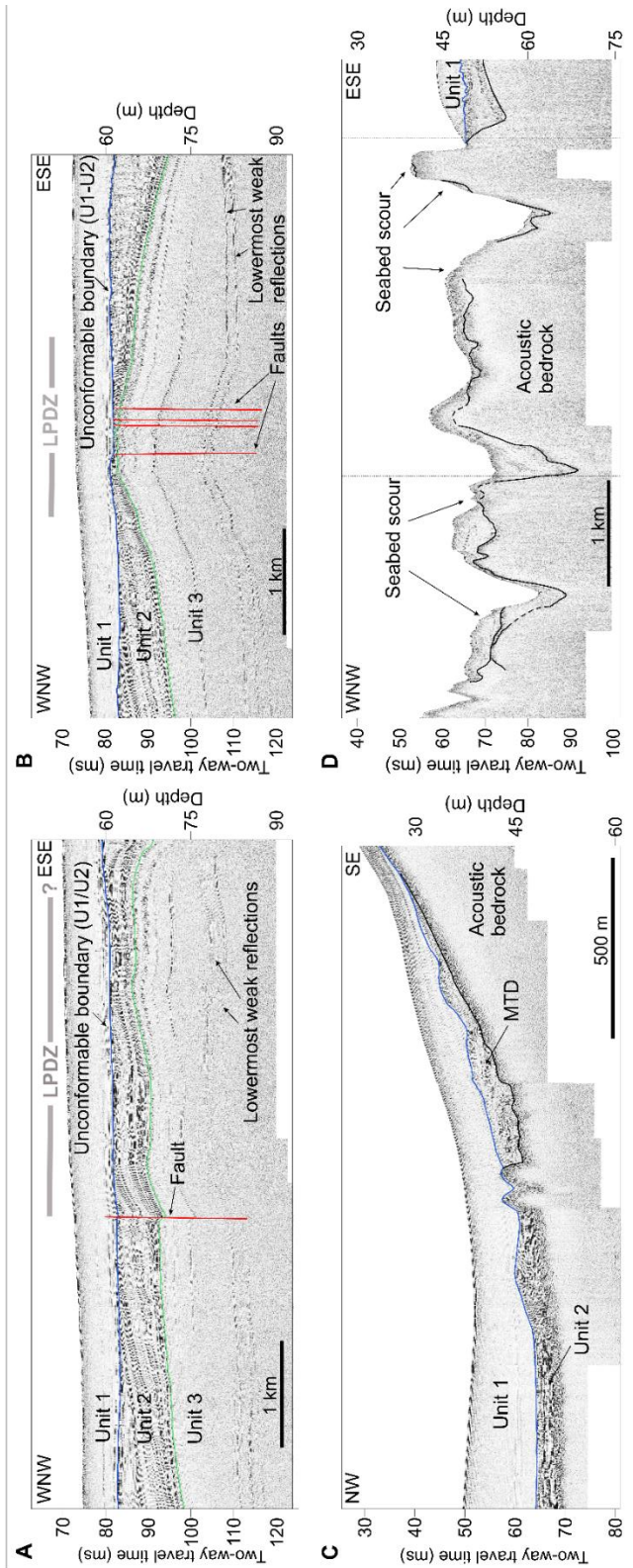




442

443 **Figure 9.** A map shows tracklines of high-resolution shallow seismic survey (black lines) with highlighted parts of the  
 444 profiles presented in **Figure 10** (yellow lines), recognized sub-bottom faults on the seismic sections projected to the surface  
 445 (red crosses) and MTD i.e, underwater landslide extent (green lines).

446 The sedimentary sequence of the Rijeka Bay shown in the seismic profiles can be divided into three  
 447 major seismic units (**Figure 10**). The upper seismic unit (Unit 1) is acoustically homogenous and semi-  
 448 transparent. Moderate-to-high amplitude and sub-parallel internal reflectors characterize the lower unit  
 449 (Unit 2). Unit 1 and Unit 2 are separated with a high amplitude unconformity. Lowermost unit (Unit  
 450 3) exhibits sub-parallel reflectors with weak amplitudes.



451

452 **Figure 10.** High-resolution seismic profiles showing **A)** Fault at the western margin of the Late Pleistocene deformation  
 453 zone (LPDZ) in profile A-A' in the Rijeka Bay; **B)** Multiple faults along the central part of the LPDZ in profile B-B' in  
 454 Rijeka Bay; **C)** Downslope mass-transport deposit (MTD i.e., underwater landslide)) in the eastern part of the Bakar Bay;  
 455 **D)** Seabed in the area south of Jadranovo scoured by bottom currents, signal penetration is weaker due to the coarser grained  
 456 sediment and shallow acoustically impermeable bedrock.

457 Neotectonic deformation along the tracklines of high-resolution seismic survey are recognized only in  
458 the NE corner of the Rijeka Bay (Figure 9). Gentle folding and decimeter-scale faulting within the Late  
459 Pleistocene stratified sediments is recognized within the Late Pleistocene Deformation Zone (LPDZ;  
460 Figures 9 and 10). LPDZ is characterized by up to a few kilometers wide and up to ten meters high  
461 antiformal structures with internal gently undulating folds (hectometers wavelengths and meters  
462 amplitudes). Besides, faulting can be easily detected in multiple seismic profiles in the Rijeka Bay  
463 (Figure 10). As visible in selected seismic profiles (Figure 10) faults can be traced in acoustic unit with  
464 moderate-to-high amplitude and sub-parallel internal reflectors. The faults and folds cannot be traced  
465 in the upper acoustically semi-transparent homogenous unit. Vertical offset of the strata along the fault  
466 is less than 25 cm. A fault direction is delineated in the map as point locations of the fault marked on  
467 the tracklines (Figure 9). A supposed fault line extends from the north of the bay (Kostrena) towards  
468 the Krk Island in the south-eastern direction (Dinaric strike). Towards the Island of Krk a fault divides  
469 into 2 or 3 possible fault lines that are part of the LPDZ.

470 Furthermore, a downslope mass-transport deposit (MTD i.e., underwater landslide) was detected in the  
471 Bakar Bay. MTD unit is characterized in the seismic profiles by irregular upper reflector and chaotic  
472 internal structure (Figure 10C). The unit is overlain by acoustically homogenous and semi-transparent  
473 upper unit (Unit 1). Its extent covers most of the farthest southeastern part of the Bakar Bay (Figure  
474 10C). It can be traced on 3 profiles (Figure 10) and is delineated on the map (Figure 9).

475 Seismic profile between the Krk Island and the mainland, located in the Mala Vrata and Vinodol  
476 Channel (Figures 9 and 10D), differs from profiles in the Rijeka Bay. The sea bottom is very irregular,  
477 with evident seabed scouring and carbonate bedrock reaching surface. Sediments that overlay  
478 carbonate bedrock are generally thin or absent due to the scouring in narrow channel. South-eastern  
479 end of the profile comprises thicker sediment succession as the channel widens and enables  
480 sedimentation. Detected sediments have low to medium amplitude reflectors due to the coarser grain  
481 size. Thus, there is no evidence of neotectonic movements on the seismic profiles in the Vinodol  
482 Channel.

483

## 484 Discussion

### 485 *Indicators of neotectonic deformations in high-resolution shallow seismic* 486 *data*

487 Neotectonic deformations can be readily recognized in the Quaternary marine and lacustrine sediment  
488 successions, either as faults folds within the stratified sediments or as secondary effects such as mass-  
489 transport deposits (MTD's, e.g., Strasser et al., 2011; Wiemer et al., 2015; Moernaut et al., 2017;  
490 Wright et al., 2019; Ojala et al., 2019) i.e., underwater landslides. The recognition of such subsurface  
491 features in the investigated area (Figure 9) allows insights into the long-term neotectonic activity  
492 spanning the Late Pleistocene and Holocene.

493 The age and lithology of the recognized seismic units, at this moment, can only be assumed and  
494 correlated with other previously published studies (Juračić et al. 1998; Brunović et al., 2020) because  
495 of the lack of sediment cores collected in the Rijeka Bay. Accordingly, the lower seismic unit (Unit 2)  
496 can be interpreted as Late-Pleistocene lacustrine/riverine sediments (Figure 10). The transition from  
497 the lower unit into the upper unit (marked with erosional surface with pronounced reflector) is

498 interpreted as the Late-Pleistocene to Holocene transition while the upper seismic unit (Unit 1) is  
499 interpreted as Holocene marine sediment.

500 Neotectonic movements are recognized in the Quaternary sediment succession only in the north-  
501 easternmost part of the Rijeka Bay along the Late Pleistocene Deformation Zone (LPDZ; **Figure 10**).  
502 The LPDZ is characterized by generally Dinaric strike (NW-SE), and the deformed Late Pleistocene  
503 stratified deposits are truncated at the top (eroded) and unconformably overlain by the undeformed  
504 Holocene marine sediments (**Figure 10**).

505 Possible secondary effects of the strong earthquakes caused by the activity of still unrecognized main  
506 seismogenic faults are MTD's in the eastern part of the Bakar Bay that could be deposited during the  
507 strong earthquake induced local slope failures in the eastern part of the Bakar Bay. The slope failures  
508 are located along a recognized neotectonic fault (**Figure 12**), although the failures could be related also  
509 to non-tectonic processes along the relatively steep flanks of the bay.

510 Since the recognized LPDZ was probably not active during Holocene, it could be explained by the  
511 shifting of the activity of the orogen-parallel neotectonic faults recognized in the NW part of the same  
512 active fault zone Ilirska Bistrica–Rijeka–Vinodol–Senj (cf. Moulin et al., 2016; Figure 1B). It should  
513 be mentioned that the NW projection of the sub-bottom linear deformation zone run across the town  
514 of Rijeka, the area characterized by the anthropogenic modifications that greatly impair access to the  
515 surface geological and geomorphological data. Even if the fault is active, the slow deformations along  
516 the zone cannot be easily recognized within the basement carbonate rocks exposed on the surface  
517 (**Figure 4**). However, the surface fault in the area of Rijeka belongs to the recognized sigmoidal fault  
518 system could be related to the LPDZ. It is supposed that the seismologically modelled fault (KF1)  
519 could also be blind, since there are no sub-bottom deformations along the projection of the fault.  
520 Besides, the KF1 can be steeper near the surface and thus could fit the fault recognized on the shallow  
521 seismic images, although we show only a simple projection of the modelled fault according to the  
522 seismological data (Figure 12).

523 The fault running through flysch synclines on the island of Krk could be a SE continuation of the  
524 recognized sub-bottom fault within the LPDZ (**Figure 12**). However, the LPDZ does not have to be  
525 related to the underlying bedrock fault, although the zone is oriented predominantly along strike of the  
526 Dinaric structures, since the uppermost Pleistocene succession could be detached either from the older  
527 Quaternary sediments or from the bedrock, and deformed only above a possible shallow detachment.  
528 Ground shaking during strong pre-historical earthquakes could trigger the deformations in the Late  
529 Pleistocene stratified sediments. Unfortunately, acoustic signal of shallow seismic did not penetrate  
530 deep enough to reach neither older Pleistocene deposits nor the bedrock (**Figure 10A and B**).

531

### 532 *Pre-existing tectonic structures and the active faults*

533 The presence of all major fault types: normal, reverse and strike-slip, the large range in their  
534 orientations as well as determined structural reactivation on many of the fault planes measured on the  
535 surface imply that the investigated area has gone through several tectonic phases. This is also evident  
536 from the near surface structures in the northeastern part of the Kvarner region (**Figures 4 and 5**). It is  
537 assumed that a major detachment has been activated within the pre-orogenic Lower Cretaceous  
538 succession during the Eocene early-orogenic thin-skinned tectonic phase in the area, and that the thin-

539 skinned tectonic cover of the Adria was dissected by the inherited thick-skin faults during Oligocene  
540 to Neogene (Korbar, 2009). Thus, most of the faults formed during the main Dinaric tectonic phases  
541 could be later reactivated as a response to the shifting tectonic stress from SW-NE to S-N (Ilić and  
542 Neubauer, 2005; Žibret and Vrabc, 2016), resulting in rather complex present-day fault net (Figure  
543 6).

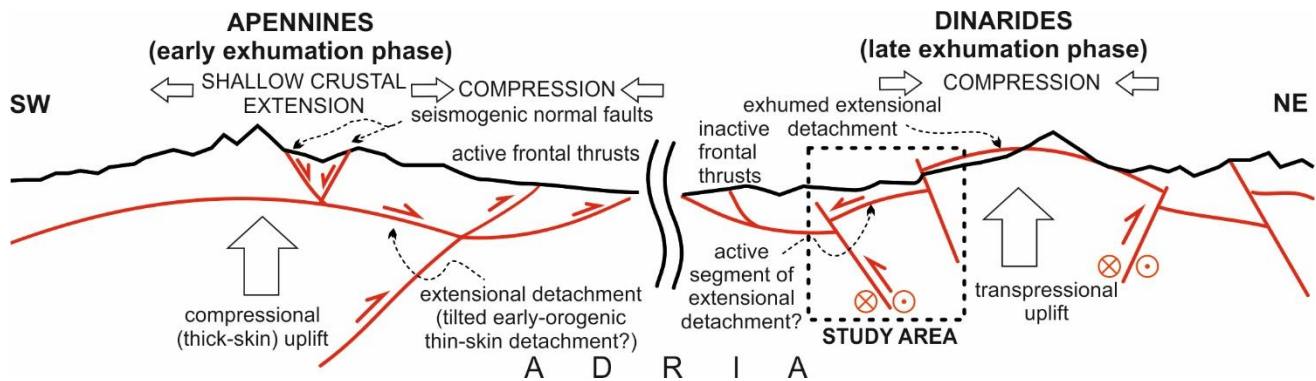
544 The steep faults mapped along the strike of the kilometre-scale Dinaric folds have been probably  
545 formed during the late-orogenic transpression (Tari, 2002; Korbar, 2009). Besides, some of the steep  
546 faults are probably near surface expression of the deep crustal active faults (Figure 8) that  
547 accommodate the tectonic escape in this part of the External Dinarides (Picha, 2002). Sigmoidal  
548 appearance of some of the possibly neotectonic strike-slip steep faults (Figure 12) could be interpreted  
549 as a shallow crustal expression of the deep crustal interaction of the active faults. Namely, the  
550 interaction of steep orogen-parallel (longitudinal) and the subvertical transversal deep active faults  
551 could result with the formation of sigmoidal (braided) arrangement of the reactivated pre-existing  
552 upper crustal faults (Figure 4). However, the along-strike displacements of the geological boundaries  
553 along the sigmoidal faults are only a few tens to a hundred meters. Thus, the displacement could be  
554 related to the neotectonic (Quaternary) deep crustal interaction of longitudinal Dinaric presumably  
555 oblique-slip (KF1 on Figure 8; Moulin et al., 2016; Žibret and Vrabc, 2016) and transversal strike-  
556 slip faults (KF2 and JFZ on Figures 4 and 8). The later could belong to the inferred Kvarner fault zone  
557 (Korbar, 2009).

558 Since the measured surface faults on the outcrops (Figure 6) do not match strictly the Fault plane  
559 solutions (FPS) calculated from the seismological data (Figure 7), it seems that both the past and the  
560 active tectonic processes are not unambiguous. Thus, the previously formed tectonic structure and the  
561 pre-existing faults in the thin-skinned tectonic cover probably do not match the deep crustal active  
562 faults (Figure 12). The tectonic movements below the thin-skinned cover could be redistributed  
563 irregularly along the near surface pre-existing faults and fractures, and thus there are no clear surface  
564 expressions of the active faults.

565 The early-orogenic detachment is supposed in the subsurface of the coastal-and-island belt (Figure 5).  
566 Theoretically, the detachment in the present-day structural setting could act as the extensional one  
567 (Korbar, 2009). The normal faults could be driven by the gravitational collapse of the thin-skinned part  
568 of the uppermost crust that tectonically overlay presumably thick-skinned and possibly still slowly  
569 growing Gorski kotar anticline along the system of deeper transpressional Dinaric faults (Figure 11).  
570 Accordingly, the near-surface structures and the pre-existing faults mapped on the surface (Figure 4),  
571 formed during the main phases of the orogenic deformations, probably only partly take over the active  
572 tectonic movements along the deeper faults. However, further research is needed for a reliable  
573 evaluation of the hypothesis.

574 The Apennines are similar but younger Alpine orogenic belt than the External Dinarides (Korbar,  
575 2009), that is also characterized by a complex interaction of the thin-skinned and thick-skinned  
576 tectonics (Butler et al., 2004; Scrocca et al., 2005; Figure 11). In central Apennines a regional almost  
577 aseismic extensional (gravitational) detachment is probably a driver for active shallow crustal normal  
578 faults that are well-known seismogenic sources of the destructive recent earthquakes in central Italy  
579 (Lavecchia et al., 2017). Seismologically weak compressional (transpressional?) thrusts are recognized  
580 below the extensional detachment at the mid-crustal depths (>20 km) where plastic deformations  
581 prevail (Finetti et al, 2001; Lavecchia et al, 2003). Thus, the thrusts could be related to the thick-skin  
582 orogenic exhumation, while the extensional detachments could be driven by the exhumational uplift of

583 the orogen (Figure 11). The extensional detachments in the late-orogenic exhumation phase could be  
 584 structurally re-arranged (tilted) early-orogenic compressional detachments (master thrusts) that  
 585 accommodated the thin-skinned tectonic deformations (cf. Korbar, 2009 for External Dinarides). In the  
 586 External Dinarides, an older counterpart of the Apennines, the orogenic exhumation reached much  
 587 shallower crustal levels, while possible seismogenic extensional detachments derived from the  
 588 structurally re-arranged (tilted) older thin-skinned compressional ones (cf. Korbar, 2009), could be  
 589 exhumed along the crest of the External Dinarides (Figure 11). If so, transpressional deformations  
 590 prevail in the upper crust of the highly exhumed External Dinarides, while the extensional tectonic  
 591 events along the presumably active remnants of the extensional detachments are possible but probably  
 592 rare (Figure 11).

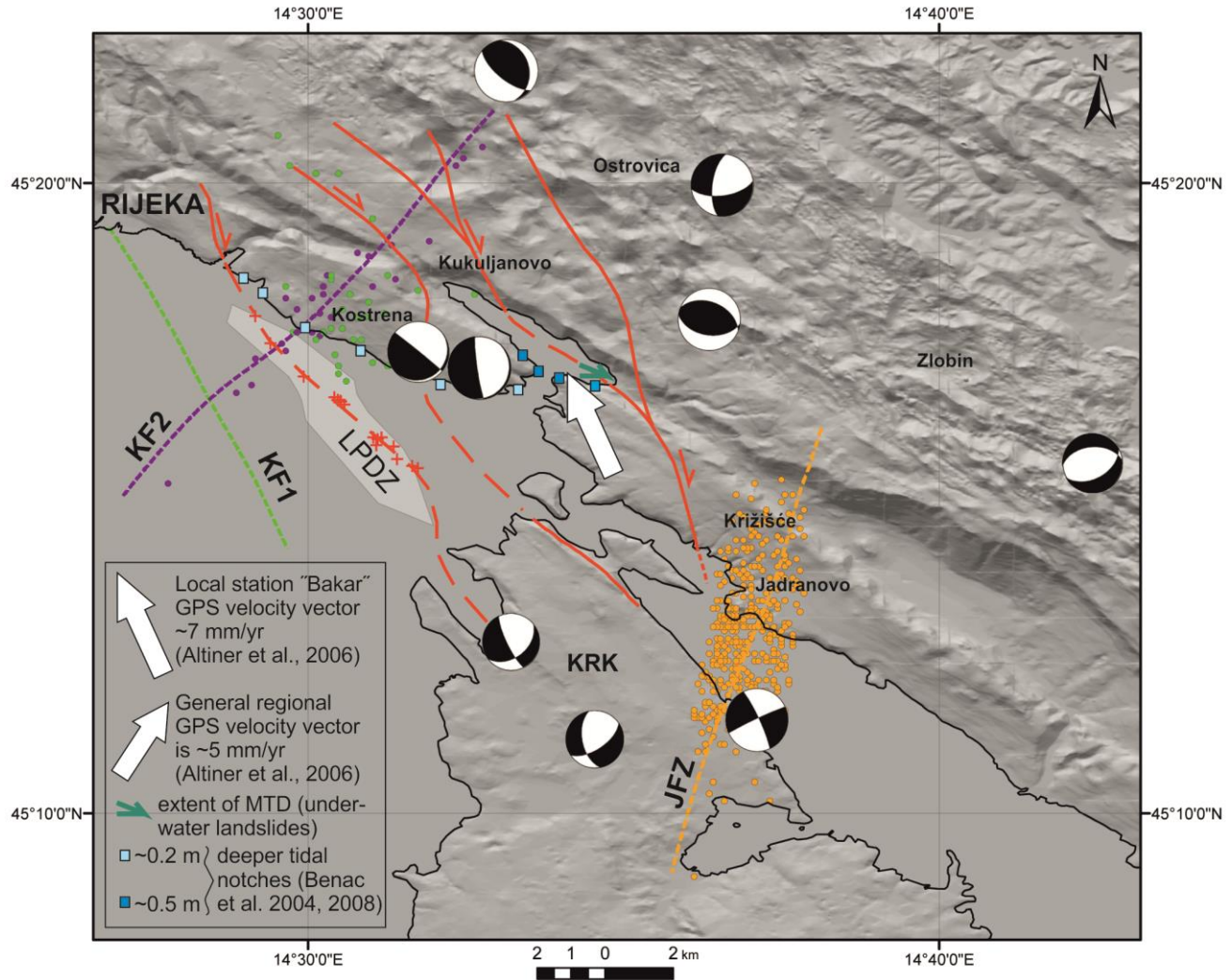


593  
 594 **Figure 11.** Comparison of the conceptual models of the present-day late orogenic exhumation phases of the two Adria  
 595 derived convergent fold-and-thrust belts: older the Dinarides and younger the Apennines.

596

### 597 *Contribution to a new seismotectonic model of the Kvarner region*

598 The existing seismotectonic model of the Kvarner region is based on 2D interpretations of a simple  
 599 projection of the selected hypocenters to the chosen cross-section (Prelogović et al., 1995; Kuk et al.,  
 600 2000). The model, among other data and analyses, is considered also for the analyses of the active  
 601 seismogenic sources in the region (Kastelic and Carafa, 2012; Kastelic et al., 2013). However, 3D  
 602 analyses of the local seismological and geological data are crucial for a reliable interpretation of the  
 603 active faults. Thus, the preliminary 3D model of the seismologically constrained deeper crustal active  
 604 faults (Figure 8) and the deformation zone interpreted according to the shallow seismic data from the  
 605 marine realm (Figures 9 and 10) are compared with the surface data (Figure 4), with the aim to make  
 606 a more relevant insight into the possible active fault regime in the investigated area Bakar-Krk (Figure  
 607 12).



608

609 **Figure 12.** Summary map of neotectonic and active faults in the investigated area Bakar-Krk. Red lines mark neotectonic  
 610 faults mapped on the surface (Figure 4) while broken red lines are their supposed submarine extensions. Shallow sub-  
 611 bottom Late Pleistocene deformation zone (LPDZ) is marked by light grey area and the related fault zone by red crosses  
 612 (see Figures 9 and 10). Colored dotted lines are surface projections of the active structures (JFZ-Jadranovo fault zone,  
 613 KF-Kostrena faults 1 and 2) modelled according to the selected hypocenters (see Figure 8). The related epicenters are  
 614 marked by dots colored as the modelled faults. The focal mechanisms (FPS “beach-balls”) are for the selected  
 615 earthquakes ( $M \geq 2.7$ ) in the wider Bakar-Krk area (see Figure 7 for details).

616 The majority of the earthquakes in the wider Rijeka epicentral area (Figure 2) are spatially distributed  
 617 generally along the strike of the External Dinarides (NW–SE) i.e., along the fault zone Ilirska Bistrica–  
 618 Rijeka–Vinodol that includes also the island of Krk (Prelogović et al., 1995; Kuk et al., 2000). The  
 619 zone comprises also the investigated Bakar area (Figure 4) that is the NW continuation of the Vinodol  
 620 fault zone (Palenik et al., 2019). The active NW-SE striking structure is regionally recognized as the  
 621 transpressional Adriatic Fault zone (Picha, 2002; Korbar, 2009; Figure 1C).

622 Many authors recognized active faults in the NW part of the External Dinarides, mostly in the SE  
 623 Slovenia (Placer et al., 2010; Kastelic and Carafa, 2012; Kastelic et al., 2013; Moulin et al., 2016).  
 624 Moulin et al. (2016) indicated three active faults some 50 kilometers NW of Rijeka that are

625 characterized by Dinaric strike and right-lateral displacement, and the active faults dissect the inactive  
626 older Dinaric thrusts. Faulting onset of the strike-slip Dinaric fault system in SE Slovenia occurred  
627 along the main fault during the Early Pliocene, while the transition from pure strike-slip to transpressive  
628 kinematics occurred during the early-middle Pleistocene. Besides, Moulin et al. (2016) found the  
629 evidence of successive activation of the parallel neighboring active faults, situated few kilometers on  
630 the south from the main fault.

631 The Late Pleistocene deformation zone (LPDZ) recognized on shallow seismic images in the NE part  
632 of the Rijeka Bay (Figure 12) is probably inactive and the activity of the related deformations could be  
633 shifted to another active fault recognized according to the seismological data. The surface projection  
634 of the fault strikes parallel to the LPDZ a few km SW (Kostrena fault 1 - KF1). If the projection would  
635 be real, it would imply that a system of parallel faults is also active in this part of the External Dinarides,  
636 and that is characterized by a shifting activity successively along neighboring (reactivated?) faults  
637 striking along the External Dinarides (NW-SE, e.g. KF1 on Figure 12). Yet, none of the fault plane  
638 solutions (FPS) of the moderate earthquakes from the area strictly match the NE dipping fault KF1,  
639 although there are the planes of the similar strike (Figure 12). It can be explained by the fact that only  
640 weak earthquakes, that are too weak for a reliable calculation of the FPS, occur along the active fault  
641 KF1. Besides, there is no recognized subsurface expression of the KF1 on the shallow seismic images  
642 of the Late Pleistocene layered sediments in that part of the Rijeka Bay (Figure 9). However, the  
643 Holocene vertical tectonic displacements could be too slow (Surić et al., 2014) to be recognized in  
644 Holocene marine sediments. Therefore, it is possible that during the Holocene ruptures occurred in this  
645 area but we do not have evidence in high-resolution shallow seismic data. Alternative explanation  
646 would be that LPDZ is not directly related to a bedrock fault, but is a consequence of possible intra-  
647 formational deformations because of possible strong prehistorical earthquake(s).

648 The instrumentally recorded seismicity in the wider Rijeka epicentral area allows analyses of only the  
649 last hundred years of the active tectonics in the region (Herak et al., 1996) while the reliable  
650 seismological data for the 3D modelling are available since 1979. It should be highlighted that  
651 historical locally destructive events occurred before the instrumental era (Herak et al., 2017). The GPS  
652 constrained ~7 mm/yr NW movement of the point situated in the SE of the Bakar Bay do not match  
653 regional ~5 mm/yr NE movement measured on other points from the Kvarner region (Altiner et al.,  
654 2006; Figure 1B). Besides, the extraordinary deep positions of the tidal notches along the southern  
655 coast of the Bakar Bay, that are ~ 0.5 m deeper than all the other notches observed elsewhere in the  
656 investigated area (Benac et al., 2004; 2006), could be related to the strange GPS vector observed on  
657 the same tectonic block (Figure 12). The prehistorical underwater landslides in the eastern part of the  
658 bay could be related to strong earthquakes in the area. Although the deeper position of the notches is  
659 previously interpreted as a results of the downthrown footwall block of the major active thrust in the  
660 Bakar Bay (Stiros and Moschas, 2012), our results cannot confirm the thrust, and the fault responsible  
661 for the possible negative displacement could be also normal (gravitational?).

662 According to the results presented in our paper, none of the seismologically defined active faults have  
663 distinct surface expression (Figure 12). The thin-skinned and highly deformed early-orogenic tectonic  
664 cover of the Adria that is illustrated on Figures 5 and 11. We supposed that active longitudinal and  
665 transversal faults dissect the Adria upper crust and cause brittle deformations and earthquakes down to  
666 approximately 20 km depths (Figure 9). Possible “blind” thrusts and strike-slip faults could be active  
667 bellow the thin-skinned tectonic cover of the Adria (Korbar, 2009). Since Adria is obviously generally  
668 moving to the north (Weber et al., 2010), a strain accumulated deeper in the crust is probably irregularly  
669 redistributed near the surface along the pre-existing fault network formed during the earlier phases of  
670 the orogenesis. The discrepancy between seismologically constrained active faults and surface geology



671 and geomorphology could be related to a complex shallow crustal anisotropy recognized generally also  
672 from the regionally differential attenuation of the seismic waves (Markušić et al., 2019). The sigmoidal  
673 strike of the generally orogen-parallel neotectonic near surface possibly active faults (Figure 12) could  
674 be related to the interaction of the deeper crustal longitudinal and transversal faults recognized in the  
675 3D model according to the seismological data (Figure 8, Supplement 1 and 2). The seismogenic faults  
676 slip could be in the uppermost crust redistributed along a rather complex network of longitudinal and  
677 transversal early-orogenic Dinaric faults (Figures 4 and 6). Thus, the active faults modelled according  
678 to the seismological data probably have a minor expression on the surface and the earthquake clusters  
679 at Kostrena and Jadranovo could appear in the area of the interaction of the deeper crustal faults (Figure  
680 12). On the overview tectonic maps, the two regional longitudinal and transversal fault zones could be  
681 generally recognized as the Northeast Adriatic and Kvarner fault zones, respectively (Korbar, 2009).  
682 However, the seismogenic faults along the zones are probably related only to the longitudinal  
683 earthquake zone Rijeka-Senj (Figure 2), since possible present-day activity along the transversal  
684 Kvarner fault zone is generally oriented parallel to the principal NE-SW present-day tectonic stress in  
685 the area (Figure 7), implying that the active faults must not be seismogenic. Thus, the geometry and  
686 position of the seismogenic faults responsible for the locally destructive historical earthquakes is still  
687 open.

688 The analyzed data did not allow a recognition of any major seismogenic fault in the subsurface of the  
689 investigated area. However, the Dinaric reverse faults that in the present-day stress field probably act  
690 as the transpressional faults could be responsible for the major historical earthquakes (Figure 11). Yet,  
691 considering theoretical large-scale normal faulting above the structurally re-arranged early-orogenic  
692 detachment that is supposed in this part of the External Dinarides (Korbar, 2009), there is also a  
693 possibility that seismogenic historical earthquakes resulted from possible large-scale gravitational  
694 displacements that are much less frequent than instrumentally recorded predominantly transpressional,  
695 reverse, oblique and strike-slip events.

696 Thus, the historical strong earthquakes (Herak et al., 2017) could also be characterized by other  
697 mechanism than instrumentally recorded. If so, the strongest historical events characterized by a  
698 centennial recurrence could be related to such an inferred kinematics that, along with the strong pre-  
699 historical tectonics recognized in the Late Pleistocene sediments, could represent a significant  
700 contribution to the long-term seismic hazard assessment for the wider Rijeka epicentral area. More  
701 than 350.000 inhabitants and the strategic National and central European infrastructure in the Rijeka  
702 area are the best motivation for further studies on the seismic hazard, that partly should be based on  
703 the results of this research.

704

### 705 *Open questions and future research*

706 Considering the open questions, further research is needed for relevant evaluation of the hypothesis.  
707 The research should be extended also onshore, when the high-resolution geomorphological data will  
708 be available. However, substantial anthropogenic modification significantly changed the  
709 geomorphology, as observed on orthophoto images of the key-areas. Yet, focused detailed  
710 geomorphological analyses of a high-resolution digital elevation model could be useful for detection  
711 of possible small-scale surface ruptures. Quaternary deposits in the area are mostly preserved within  
712 the marine and lacustrine basins, and focused high-resolution bathymetric and shallow seismic survey

713 is needed for more precise definition of the recognized sub-bottom structures and for the detection of  
714 possible similar deformations in the areas that are not covered by the presented research.

715 Quaternary deposits on shore are relatively scarce, especially those of MIS 5e age that are often used  
716 as indicators of tectonic activity in other areas (e.g., Lambeck et al., 2004). Besides, possible Holocene  
717 deposits along the shorelines could be important for future studies on active tectonic. Furthermore,  
718 reported marine sediments onshore on the island of Krk should be re-investigated (Marjanac et al.,  
719 1993). It would be useful also to focus on the micro-environmental influence on the morphology of the  
720 tidal notches, that are regarded as geomorphological indicators of the vertical tectonic movements. It  
721 is especially important for specific marine environments such is the Bakar Bay, that is characterized  
722 by the tidal notches at the lowest position in respect to the notches around the Kvarner Bay (Benac et  
723 al., 2004, 2008).

724 We have not addressed the alternative causes of the registered small-scale seismicity clustered along  
725 the sub-vertical transversal zones that are used for the 3D modelling of the active faults in the area.  
726 The strange orientation of the cluster and depth range from the subsurface to up to 25 km could be  
727 related also to the changes in the pore fluid conditions, influenced by larger-scale NW-SE oriented  
728 faults. Such fluid conduits, changes in the fluid recharge and the related changes in the pore pressure  
729 can cause poroelastic stressing of the surrounding rocks leading to local stress perturbations and  
730 possible induced seismicity (e.g. Parotidis et al., 2003; Talwani et al., 2007). This may explain at least  
731 some of the registered events, but more detailed and structured work is needed for a more substantial  
732 interpretation.

734 Analyses of the GPS velocities at the carefully selected points that should be defined also according to  
735 the results of the presented research is crucial for future studies of the already generally recognized  
736 differential movements of the tectonic blocks in the area. Thus, GPS constrained movements of the  
737 specific points on the both sides of the supposed neotectonic faults should be observed in future  
738 research.

739 All the aforementioned research could be performed during the inter-seismic period, while the  
740 unwanted but possible strong seismic events should be followed by the application of differential  
741 interferometric synthetic aperture radar technique or other up-to-date geodetic methods that can detect  
742 co-seismic displacements along still undefined active faults in the wider Rijeka epicentral area.

743

744

## 745 **Conclusions**

746

747 In the investigated part of the Kvarner region (Bakar-Krk area), coastal-and-island belt is built of the  
748 kilometre-scale tightly folded pre-orogenic successions of Lower Cretaceous to Paleogene carbonates  
749 and flysch rocks. The tight folds appear probably above an early-orogenic thin-skinned detachment  
750 that was formed during the main tectonic phase in this part of the External Dinarides (Eocene). The  
751 thin-skinned belt is in a major tectonic contact with the huge Gorski kotar anticline that could be  
752 considered as a contemporaneous or later thick-skin structure (Oligocene). The steep faults mapped

753 along strike of the kilometre-scale Dinaric folds have been probably formed during the late-orogenic  
754 (Oligocene-Miocene) transpression. The presence of normal, reverse and strike-slip faults, the large  
755 range in their orientations as well as determined structural reactivation on many of the fault planes  
756 imply that the investigated area has gone through several tectonic phases of the long-lasting Alpine-  
757 type orogenesis that in the region resulted with the formation of the External Dinarides fold-and-thrust  
758 belt.

759 The calculated focal mechanisms of the moderate recent instrumentally recorded earthquakes in the  
760 investigated region imply the prevailing reverse deformation on generally NW-SE oriented faults,  
761 undetermined strike slip solutions, and a few events also giving evidence for normal faulting along  
762 variously oriented planes. All of the solutions are generally compatible with the regional NE-SW  
763 oriented principal present-day stress direction and testify to a long-term convergent tectonic setting at  
764 the Adria – Eurasia margin.

765 The spatial and temporal distribution of hypocenters of the selected instrumentally recorded weak  
766 earthquake clusters indicate predominantly subvertical transversal (NE-SW and NNE-SSW) deep  
767 crustal active faults in the investigated area. Besides, a steeply NE dipping active fault characterized  
768 by the Dinaric strike (NW-SE) is indicated as well.

769 The Adria moves generally northward, and a strain accumulating deeper in the crust could be released  
770 along the blind faults that have not a clear surface expression. The active tectonic movements deeper  
771 in the crust are probably irregularly redistributed near the surface along the pre-existing fault net  
772 formed during the earlier phases of the orogenesis. Thus, the braided system of possibly active  
773 neotectonic steep faults characterized by a sigmoidal strike could be near surface expression of the  
774 deep crustal interaction of the active longitudinal (orogen-parallel) and transversal faults in the area  
775 that probably accommodate the tectonic escape in this part of the External Dinarides.

776 In the northeastern part of the Rijeka Bay the deformations in the Late Pleistocene stratified sediments  
777 could imply pre-historical activity of a fault characterized by the Dinaric strike (NW-SE). However,  
778 Holocene transgressive marine sediments are not deformed but unconformably overlay eroded Late  
779 Pleistocene deposits. The nearby parallel active fault modelled from the seismological data (KF1) could  
780 imply a shifting of the tectonic activity among the neighboring faults in the investigated area, although  
781 the modelled fault could also be blind, since there are no sub-bottom deformations along the surface  
782 projection of the fault. However, the LPDZ does not have to be dissected by the underlying bedrock  
783 fault, since the uppermost Pleistocene succession could be detached either from the older Quaternary  
784 sediments or from the bedrock, and deformed because of shaking caused by possible strong pre-  
785 historical earthquakes.

786 There are no distinct surface traces of the modelled active faults in the investigated part of the Kvarner  
787 region. Thus, the active faults in the coastal-and-island belt are possibly situated below the thin-skinned  
788 and highly deformed shallow crustal tectonic cover of the Adria. Regarding the supposed model, a new  
789 conceptual comparison of the late orogenic evolution of the External Dinarides with the much better  
790 explored Apennines is presented.

791

792 Our aim is to create a robust inventory of multidisciplinary data that will be continuously updated and  
793 will serve for the purposes of identification and parametrization of active faults in the Kvarner region.  
794 Up to now we populated it with data from focused geological mapping, shallow seismic profiles of the

795 off-shore sector, the compilation of focal mechanism solutions for relatively stronger earthquakes in  
796 the area, and made a preliminary attempt in trying to fit the hypocenters of the recent relatively well  
797 located events. While our results do not discuss from the already established seismotectonic  
798 characteristics of the area, they on the other hand offer more detail and possibly a clearer insight on the  
799 role of steep fault planes that seem to cut across the region along prevailing NW-SE oriented typical  
800 Dinaric geomorphological and geological features.

801

802

### 803 **Author Contribution**

804 TK coordinated the multidisciplinary research and conceptually formatted the paper, provided a  
805 geological background and lead the interpretation of the results. SM performed the analysis of  
806 seismicity and prepared fault-plane solutions for the selected events. OH and DB were responsible for  
807 high-resolution shallow seismic data acquisition and interpretation. LF coordinated the geological  
808 mapping and prepared geological cross-sections. NB handled the spatial data, prepared the background  
809 maps and is responsible for the 3D fault modelling according to the selected hypocenters from the  
810 database. DP prepared the structural-geological analyses and contributed to the geological  
811 interpretations. VK contributed to the critical discussion on the regional seismotectonic setting and  
812 seismogenic sources and participated in the manuscript writing and review. All the authors contributed  
813 to the paper in the parts related to their expertise and provided critical feedback for the discussion.

814

815

### 816 **Acknowledgments**

817 This work has been supported by Croatian Science Foundation under the project GEOSEKVA (HRZZ  
818 IP-2016-06-1854) and partly is the result of training and education conducted through GeoTwinn  
819 project that has received funding from the European Union's Horizon 2020 research and innovation  
820 program under grant agreement No. 809943. We thank to other members of GEOSEKVA geological  
821 mapping team: Vlatko Brčić, Marko Budić and Marko Špelić, for contribution to the fieldwork. We  
822 would like to thank to two anonymous reviewers and especially to the Editor Nathan Toke for very  
823 constructive suggestions used for improvement of an earlier version of the manuscript.

824

### 825 **References**

826 Altiner, Y., Bačić, Ž., Bačić, T., Coticchia, A., Medved, M., Mulić, M., and Nurçe, B., 2006. Present  
827 day tectonics in and around the Adria plate inferred from GPS measurements. In Dilek, Y., Pavlides,  
828 S. (Eds.), Postcollisional tectonics and magmatism in the Mediterranean region and Asia. Geological  
829 Society of America Special Paper 409, 43–55.

830 Acta Buccarana, dokumenti za 1751–1763, signature A.91.196.174.276.663.; HR-HDA-21, Serije A,  
831 kutije 8, 10, 11 and 17, Hrvatski državni arhiv, Zagreb.

- 832 Anderson, H. A. and Jackson, J. A. (1987). Active Tectonics of the Adriatic Region. *Geophys. J. R.*  
833 *Astron. Soc.* 91, 937–983.
- 834 Angelier, J. and Mechler, P. (1977). Sur une méthode graphique de recherche des contraintes  
835 principales également utilisable en tectonique et en séismologie: La méthode des dièdres droits. *Bull.*  
836 *Soc. Géol. France* 19, 1309–1318, doi:10.2113/gssgfbull.S7-XIX.6.1309.
- 837 Battaglia, M., Murray, M.H., Serpelloni, E. and Bürgmann, R. (2004). The Adriatic region: An  
838 independent microplate within the Africa-Eurasia collision zone. *Geophysical Research Letters* 31, 1–  
839 4, doi: 10.1029/2004GL019723.
- 840 Benac, Č. and Juračić, M. (1998). Geomorphological indicators of the sea-level changes during upper  
841 Pleistocene (Wuerm) and Holocene in the Kvarner region. *Acta Geographica Croatica* 33, 27– 45.
- 842 Benac, Č., Juračić, M., Bakran-Petricioli, T. (2004). Submerged tidal notches in the Rijeka Bay NE  
843 Adriatic Sea: indicators of relative sea-level change and of recent tectonic movements. *Marine Geology*  
844 212, 21–33.
- 845 Benac, Č., Juračić, M., Blašković, I. (2008). Tidal notches in Vinodol Channel and Bakar Bay, NE  
846 Adriatic Sea: indicators of recent tectonics. *Marine Geology* 248, 151–160.  
847 <http://dx.doi.org/10.1016/j.margeo.2007.10.010>
- 848 Benjamin, J., Rovere, A., Fontana, A., Furlani, S., Vacchi, M., Inglis, R.H., Galili, E., Antonioli, F.,  
849 Sivan, D., Miko, S., Mourtzas, N., Felja, I., Meredith-Williams, M., Goodman-Tchernov, B., Kolaiti,  
850 E., Anzidei, M., Gehrels, R. (2017). Late Quaternary sea-level changes and early human societies in  
851 the central and eastern Mediterranean Basin: an interdisciplinary review. *Quat. Int.* 449, 29–57,  
852 <https://doi.org/10.1016/j.quaint.2017.06.025>.
- 853 Brunović, D., Miko, S., Hasan, O., Papatheodorou, G., Ilijanić, N., Miserocchi, S., Correggiari, A.  
854 and Geraga, M. (2020). Late Pleistocene and Holocene paleoenvironmental reconstruction of a  
855 drowned karst isolation basin (Lošinj Channel, NE Adriatic Sea). *Palaeogeography,*  
856 *Palaeoclimatology, Palaeoecology* 554, 109587. <https://doi.org/10.1016/j.palaeo.2020.109587>
- 857 Butler, R. W. H., Mazzoli, S., Corrado, S., De Donatis, M., Di Bucci, D., Gambini, R., Naso, G.,  
858 Nicolai, C., Scrocca, D., Shiner, P. and Zucconi V. (2004). Applying thick-skinned tectonic models  
859 to the Apennine thrust belt of Italy—Limitations and implications, in K. R. McClay, ed., *Thrust*  
860 *tectonics and hydrocarbon systems.* AAPG Memoir 82, 647– 667.
- 861 Correggiari, A., Roveri, M., Trincardi, F. (1996). Late Pleistocene and Holocene Evolution of the  
862 North Adriatic Sea. *II Quaternario* 9. 697–704.
- 863 Cunningham, D., Grebby, S., Tansey, K., Gosar, A., and Kastelic, V. (2006). Application of airborne  
864 LiDAR to mapping seismogenic faults in forested mountainous terrain, southeastern Alps, Slovenia,  
865 *Geophys. Res. Lett.*, 33, L20308, doi:10.1029/2006GL027014.
- 866 Daxer, C., Sammartini, M., Molenaar, A., Piechl, T., Strasser, M. and Moernaut, J. (2019).  
867 Morphology and spatio-temporal distribution of lacustrine mass-transport deposits in Wörthersee,  
868 Eastern Alps, Austria. *Geological Society London Special Publications.* doi: 10.1144/SP500-2019-  
869 179

- 870 Finetti, I.R., Boccaletti, M., Bonini, M., Del Ben, A., Geletti, R., Pipan, M. and Sani, F. (2001).  
 871 Crustal section based on CROP seismic data across the North Tyrrhenian–Northern Apennines–  
 872 Adriatic Sea. *Tectonophysics* 343, 135–163.
- 873 Fuček, L., Matičec, D., Vlahović, I., Oštrić, N., Prtoljan, B., Korolija B., Korbar, T., Husinec, A. and  
 874 Palenik, D. (2015). Osnovna geološka karta Republike Hrvatske mjerila 1:50.000 – list Cres i Lošinj  
 875 (Basic Geological Map of the Republic of Croatia 1:50.000 Scale – Cres and Lošinj sheet). Hrvatski  
 876 geološki institut, Zavod za geologiju, ISBN: 978-953-6907-53-3, Zagreb.
- 877 Gratianus, X. (1755). De usu Mercurii tam externe quam interne usurpati: observationes medico-  
 878 practicae cum animadversionibus et ad calcem epicrisis, Viennae Austriae MDCCLV Ex typographia  
 879 Kaliwodiana, p 179.
- 880 Gülerce, Z., Šalić, R., Kuka, N., Markušić, S., Mihaljević, J., Kovačević, V., Sandikkaya, A.,  
 881 Milutinović, Z., Duni, L., Stanko, D., Kaludjerović, N. and S. Kovačević: Seismic hazard maps for the  
 882 Western Balkan. *Inženjerstvo okoliša*, 4/1, 2017, 7-17.
- 883 Herak, M. (1980). Sustav navlaka između Vrbovskog i Delnica u Gorskom kotaru (The nappe-system  
 884 between Vrbovsko and Delnice in Gorski kotar (Croatia). *Acta Geologica* 10/2, 35–51, Zagreb.
- 885 Herak, M., Herak, D., and Markušić, S. (1996). Revision of the earthquake catalogue and seismicity of  
 886 Croatia, 1908-1992. *Terra Nova* 8, 86–94.
- 887 Herak, D., Sović, I., Cecić, I., Živčić, M., Dasović, I. and Herak M. (2017). Historical seismicity of the  
 888 Rijeka region (NW External Dinarides, Croatia) - Part I: Earthquakes of 1750, 1838 and 1904 in the  
 889 Bakar epicentral area. *Seismol. Res. Lett.* 88/3, 904–915.
- 890 HGI (2009). Geological map of the Republic of Croatia in scale 1:300.000. Hrvatski geološki institut  
 891 - Croatian Geological Survey, available at <http://webgis.hgi-cgs.hr/gk300/default.aspx>
- 892 Ilić, A. and Neubauer, F. (2005). Tertiary to recent oblique convergence and wrenching of the Central  
 893 Dinarides: Constraints from a palaeostress study. *Tectonophysics* 410, 465–484.
- 894 Ivančić, I., Herak, D., Markušić S., Sović, I. and Herak, M. (2006). Seismicity of Croatia in the period  
 895 2002–2005. *Geofizika* 23, 87–103.
- 896 Ivančić, I., Herak, D., Herak, M., Allegretti, I., Fiket, T., Kuk, K., Markušić, S., Prevolnik, S. Sović,  
 897 I., Dasović, I. and Stipčević J. (2018). Seismicity of Croatia in the period 2006–2015. *Geofizika*, 35,  
 898 69–98.
- 899 Juračić, M., Crmarić, R. and Benac, Č. (1998). Holocenski sedimenti i sedimentacija u Riječkom  
 900 zaljevu, in: Arko-Pijevac, M., Kovačić, M. & Crnković, D. (eds.), *Prirodoslovna istraživanja riječkog*  
 901 *područja. Prirodoslovna biblioteka* 1, 339–344, Prirodoslovni muzej Rijeka.
- 902 Juračić, M., Benac, Č. and Crmarić, R. (1999). Seabed and surface sediments map of the Kvarner  
 903 Bay, Adriatic Sea, Croatia (Lithological map, M 1:500,000). *Geologia Croatica* 52, 131–140.
- 904 Kastelic, V. and Carafa, M.M.C. (2012). Fault slip rates for the active External Dinarides thrust-and-  
 905 fold belt. *Tectonics* 31, TC3019, doi:10.1029/2011TC003022.

- 906 Kastelic, V., Vannoli, P., Burrato, P., Fracassi, U., Tiberti, M.M. and Valensise, G. (2013).  
907 Seismogenic sources in the Adriatic Domain. *Mar. Petrol. Geol.* 42, 191–213. doi:  
908 10.1016/j.marpetgeo.2012.08.002.
- 909 Kišpatić, M. (1891). Šesto i sedmo izvješće potresnoga odbora za godine 1888.-1889. Rad  
910 Jugoslavenske akademije znanosti i umjetnosti. Matematičko-prirodoslovni razred, knj. 11.
- 911 Korbar, T. (2009). Orogenic evolution of the External Dinarides in the NE Adriatic region: a model  
912 constrained by tectonostratigraphy of Upper Cretaceous to Paleogene carbonates. *Earth-Science*  
913 *Reviews* 96, 296–312.
- 914 Kuk, V., Prelogović, E. and Dragičević, I. (2000). Seismotectonically Active Zones in the Dinarides.  
915 *Geologia Croatica* 53/2, 295-303.
- 916 Lambeck, K., Antonioli, F., Purcell, A. and Silenzi, S. (2004). Sea-level change along the Italian coast  
917 for the past 10,000 yr. *Quaternary Science Reviews* 23, 1567-1598.
- 918 Lambeck, K., Antonioli, F., Anzidei, M., Ferranti, L., Leoni, G., Scicchitano, G. and Silenzi, S.  
919 (2011). Sea level change along the Italian coast during the Holocene and projections for the future.  
920 *Quat. Int.* 232, 250–257. <https://doi.org/10.1016/j.quaint.2010.04.026>.
- 921 Laszowski, E. (1923). Gorski Kotar i Vinodol. Matica Hrvatska, Tiskara “Narodnih novina”, Zagreb,  
922 p 264.
- 923 Lavecchia, G., Boncio, P. and Creati, N. (2003). A lithospheric-scale seismogenic thrust in central  
924 Italy. *Journal of Geodynamics* 36, 79–94.
- 925 Lavecchia, G., G. M. Adinolfi, R. de Nardis, F. Ferrarini, D. Cirillo, F. Brozzetti, R. De Matteis, G.  
926 Festa and Zollo, A.(2017). Multidisciplinary inferences on a newly recognized active east-dipping  
927 extensional system in Central Italy. *Terra Nova* 29, 77–89, doi:10.1111/ter.12251.
- 928 Marjanac, Lj., Poje, M. and Marjanac, T. (1993). Pleistocene marine and terrestrial sediments with  
929 striata fauna on the island of Krk. *Rad Hrvatske akademije znanosti i umjetnosti* 463, 49-62, Zagreb.
- 930 Markušić, S., Stanko, D., Korbar, T. and Sović, I. (2019). Estimation of near-surface attenuation in the  
931 tectonically complex contact area of the northwestern External Dinarides and the Adriatic foreland.  
932 *Nat. Hazards Earth Syst. Sci.* 19, 2701–2714.
- 933 Markušić, S. Stanko, D., Korbar T., Belić, N., Penava, D. and Kordić, B. (2020). The Zagreb  
934 (Croatia) M5.5 Earthquake on 22 March 2020. *Geosciences* 10, 252.
- 935 Marrett, R. and Allmendinger, R.W. (1990). Kinematic analysis of fault-slip data. *Journal of*  
936 *Structural Geology* 12, 973–986. doi:10.1016/0191-8141(90)90093-E.
- 937 Moernaut, J., Van Daele, M., Strasser, M., Clare, M., Heirman, K., Viel, Cardenas, J., Kilian, R.,  
938 Ladrón de Guevara, B., Pino, M., Urrutia, R. and De Batist, M. (2017). Lacustrine turbidites  
939 produced by surficial slope sediment remobilization: A mechanism for continuous and sensitive  
940 turbidite paleoseismic records. *Marine Geology* 384, 159–176.

- 941 Missiaen, T., Slob, E. and Donselaar, M.E. (2008). Comparing different shallow geophysical  
 942 methods in a tidal estuary, Verdrongen Land van Saeftinge, Western Scheldt, the Netherlands.  
 943 Netherlands Journal of Geosciences *Geologie en Mijnbouw* 87 (2), 151–164
- 944 Moulin, A., Benedetti, L., Rizza, M., Jamšek Rupnik, P., Gosar, A., Bourlès, D, Keddadouche, K.,  
 945 Aumaître, G., Arnold, M., Guillou, V. and Ritz, J.F. (2016). The Dinaric fault system: Large-scale  
 946 structure, rates of slip, and Plio-Pleistocene evolution of the transpressive northeastern boundary of the  
 947 Adria microplate, *Tectonics*, 35, 2258–2292 doi:10.1002/2016TC004188.
- 948 Nocquet, J-M. and Calais, E. (2004). Geodetic Measurements of Crustal Deformation in the Western  
 949 Mediterranean and Europe. *Pure appl. geophys.* 161, 661–681, doi: 10.1007/s00024-003-2468-z.
- 950 Ojala, A.,E.,K., Mattila, J., Hämäläinen, J. and Sutinen, R. (2019). Lake sediment evidence of  
 951 paleoseismicity: Timing and spatial occurrence of late- and postglacial earthquakes in Finland.  
 952 *Tectonophysics* 771, 228–227.
- 953 Oldow, J.S., Ferranti, L., Lewis, D.S., Campbell, J.K., D'Argenio, B., Catalano, R., Pappone, G.,  
 954 Carmignani, L., Conti, P. and Aiken, C.L.V. (2002). Active fragmentation of Adria, the north African  
 955 promontory, central Mediterranean region. *Geology* 30/9, 779–782.
- 956 Ortner, H., Reiter, F. and Acs, P. (2002). Easy handling of tectonic data: The programs TectonicVB  
 957 for Mac and Tectonics FP for Windows™. *Computers and Geosciences* 28, 1193–1200.
- 958 Palenik, D., Matičec, D., Fuček, L., Matoš, B., Herak, M. and Vlahović, I. (2019). Geological and  
 959 structural setting of the Vinodol Valley (NW Adriatic, Croatia): insights into its tectonic evolution  
 960 based on structural investigations. *Geologia Croatica* 72/3, 179-193, doi: 10.4154/gc.2019.13.
- 961 Parotidis, M., Rothert, E. and Shapiro, S. A. (2003). Pore-pressure diffusion: A possible triggering  
 962 mechanism for the earthquake swarms 2000 in Vogtland/NW-Bohemia, central Europe. *Geophys. Res.*  
 963 *Lett.* 30(20), 2075, doi:10.1029/2003GL018110.
- 964 Perrey, A. (1850). Memoire sur les tremblements de terre ressentis dans la Peninsule turco-hellenique  
 965 et en Syrie, Mémoires couronnées et mémoires des savants etrangers. Publiées par l'Académie royale,  
 966 Tome XXIII, Bruxelles.
- 967 Picha, F.J. (2002). Late orogenic strike-slip faulting and escape tectonics in frontal Dinarides-  
 968 Hellenides, Croatia, Yugoslavia, Albania and Greece. *AAPG Bulletin* 86/9, 1659–1671.
- 969 Placer, L., Vrabec, M., and Celarc, B. (2010). The bases for understanding of the NW Dinarides and  
 970 Istria Peninsula tectonics. *Geologija* 53/1, 55–86, DOI 10.5474/geologija.2010.005.
- 971 Prelogović, E., Kuk, V., Jamičić, D., Aljinović, B. and Marić, K. (1995). Seizmotektonska aktivnost  
 972 Kvarnerskog područja. In: I. Vlahović, I. Velić, M. Šparica (Eds), Proceedings of the First Croatian  
 973 Geological Congress, vol. 2, Croatian Geological Society and Institute of Geology, Opatija, 487–490.
- 974 Radics, P. (1903). Geschichtliche Erinnerungen an das grosse Erdbeben in Fiume im Jahre 1750.  
 975 Sonderabdruck aus der Monatsschrift „Die Erdbebenwarte“, Nr. 11 and 12, II. Jahrg., 1–7, Laibach,  
 976 Druck von Ig. v. Kleinmayr & Fed. Bamberg.
- 977 Savić, D. and Dozet, S. (1985). Osnovna geološka karta SFRJ 1: 100.000: List Delnice (Basic  
 978 geological map of SFRY: Sheet Delnice) L 33-90. Geološki zavod; OOUR za geologiju i



- 979 paleontologiju, Zagreb; Geološki zavod, Ljubljana (1970.-1983). Savezni geološki institut, Beograd,  
980 1984.
- 981 Schmid, S.M., Bernoulli, D., Fügenschuh, B., Matenco, L., Schefer, S., Schuster, R., Tischler, M. and  
982 Ustaszewski, K. (2008). The Alps-Carpathians-Dinarides-connection: a correlation of tectonic units.  
983 *Swiss J. Geosci* 101, 139–183.
- 984 Scrocca, D., Carminati, E., Doglioni, C. (2005). Deep structure of the southern Apennines, Italy: thin  
985 skinned or thick-skinned? *Tectonics* 24/3, 1–20.
- 986 Stipčević, J., Herak, M., Molinari, I., Dasović, I., Tkalčić, H., and Gosar, A. (2020). Crustal thickness  
987 beneath the Dinarides and surrounding areas from receiver functions. *Tectonics* 39,  
988 <https://doi.org/10.1029/2019TC005872>.
- 989 Stiros, S.C. and Moschas, F. (2012). Submerged notches, coastal changes and tectonics in the Rijeka  
990 area, NW Croatia. *Marine Geology* 329, 103–112.
- 991 Strasser, M., Moore, G., Kimura, G., Kopf, A., Underwood, M. and Guo, J. (2011). Slumping and  
992 mass transport deposition in the Nankai fore arc: Evidence from IODP drilling and 3D reflection  
993 seismic data. *Geochemistry, Geophysics, Geosystems*, 12/5.
- 994 Surić, M., Juračić, M., Horvatinčić, N. and Krajcar Bronić, I. (2005). Late Pleistocene-Holocene sea-  
995 level rise and the pattern of coastal karst inundation: records from submerged speleothems along the  
996 Eastern Adriatic Coast (Croatia). *Mar. Geol.* 214, 163–175.  
997 <https://doi.org/10.1016/j.margeo.2004.10.030>.
- 998 Surić, M., Korbar, T. and Juračić, M. (2014). Tectonic constraints on the late Pleistocene-Holocene  
999 relative sea-level change along the north-eastern Adriatic coast (Croatia). *Geomorphology* 220, 93–  
1000 103.
- 1001 Šikić, D., Polšak, A. and Magaš, N. (1969). Osnovna geološka karta SFRJ 1:100.000, list Crikvenica  
1002 (Basic Geological Map of SFRY 1:100.000 Scale, Crikvenica Sheet) L 33–101. *Inst. geol. istraž.*  
1003 *Zagreb (1958–1967), Sav. geol. zavod Beograd.*
- 1004 Šikić, D., Pleničar, M. and Šparica, M. (1972). Osnovna geološka karta SFRJ 1:100.000, list Ilirska  
1005 Bistrica (Basic Geological Map of SFRY 1:100.000 Scale, Ilirska Bistrica Sheet) L 33–89. *Inst. geol.*  
1006 *istraž. Zagreb (1958–1967), Sav. geol. zavod Beograd.*
- 1007 Šumanovac, F., Markušić, S., Engelsfeld, T., Jurković, K. and Orešković, J. (2017). Shallow and deep  
1008 lithosphere slabs beneath the Dinarides from teleseismic tomography as the result of the Adriatic  
1009 lithosphere downwelling. *Tectonophysics* 712–713, 523-541, doi: 10.1016/J.Tecto.2017.06.018.
- 1010 Šušnjar, M., Bukovac, J., Nikler, L., Crnolatac, I., Milan, A., Šikić, D., Grimani, I., Vulić, Ž. and  
1011 Blašković, I. (1970). Osnovna geološka karta SFRJ 1:100.000, list Crikvenica (Basic Geological Map  
1012 of SFRY 1:100.000 Scale, Crikvenica Sheet) L 33–102. *Inst. geol. istraž. Zagreb (1961–1969), Sav.*  
1013 *geol. zavod Beograd.*
- 1014 Talwani, P., Chen, L. and Gahalaut, K. (2007). Seismogenic permeability, *ks, J. Geophys. Res.* 112,  
1015 B07309, doi:10.1029/2006JB004665.

- 1016 Tari, V. (2002). Evolution of the northern and western Dinarides: a tectonostratigraphic approach.  
1017 European Geosciences Union, Stephan Mueller Special Publication Series 1, 223–236.
- 1018 Tomsich, V. (1886). Notizie storiche sulla città di Fiume – cronologicamente svolte, Fiume, in  
1019 Stabilimento Tipo-Litografico di, E. Mohovich (Editor), 621 pp. (in Italian).
- 1020 Žibret, L. and Vrabc, M. (2016). Paleostress and kinematic evolution of the orogeny-parallel NW–SE  
1021 striking faults in the NW External Dinarides of Slovenia unraveled by mesoscale fault-slip data  
1022 analysis. *Geologia Croatica* 69/3, 295–305.
- 1023 Yutsis, V., Krivosheya, K., Levchenko, O., Lowag, J., de León Gómez, H. and Tamez Ponce, A.  
1024 (2014). Bottom topography, recent sedimentation and water volume of the Cerro Prieto Dam, NE  
1025 Mexico. *Geofísica Internacional* 53/ 1, 27–38
- 1026 Unnithan, V. and Rossi, A. P. (2018). Enigmatic Holocene sand ridges: complex meandering to  
1027 anastomosing bedforms in the North Sea (GermanSeabight). *Geo-Marine Letters* 38,417–428. doi:  
1028 10.1007/s00367-018-0543-9
- 1029 Wang, F., Dong, L., Ding, J., Zhou, X., Tao, C., Lin, X. and Liang, G. (2019). An Experiment of the  
1030 Actual Vertical Resolution of the Sub-bottom Profiler in an Anechoic Tank. *Archives of acoustics*  
1031 44/ 1, 185–194. doi: 10.24425/aoa.2019.126364
- 1032 Weber, J., Vrabc, M., Pavlovčič-Prešeren, P., Dixon, T., Jiang, Y and Stopar, B. (2010). GPS-  
1033 derived motion of the Adriatic microplate from Istria Peninsula and Po Plain sites, and geodynamic  
1034 implications. *Tectonophysics* 483, 214–222.
- 1035 Wiemer, G., Moernaut, J., Stark, N., Kempf, P., De Batist, M., Pino, M., Urrutia, R., Ladrón de  
1036 Guevara, B., Strasser, M. and Kopf, A. (2015). The role of sediment composition and behavior under  
1037 dynamic loading conditions on slope failure initiation: a study of a subaqueous landslide in  
1038 earthquake-prone South-Central Chile. *Int J Earth Sci (Geol Rundsch)* 104, 1439–1457. DOI  
1039 10.1007/s00531-015-1144-8
- 1040 Winton, T. (2020). Quantifying Depth of Burial and Composition of Shallow Buried Archaeological  
1041 Material: Integrated Sub-bottom Profiling and 3D Survey Approaches, in: McCarthy, J.K., Benjamin,  
1042 J., Winton, T., van Duivenvoorde W., 3D Recording and Interpretation for Maritime Archaeology  
1043 Springer Coastal Research Library 31, 154–174, doi: 10.1007/978-3-030
- 1044 Wright, V., Hornbach, M., Brown, L., McHugh, C. and Mitchell, S. (2019). Neotectonics of  
1045 Southeast Jamaica Derived From Marine Seismic Surveys and Gravity Cores. *Tectonics* 38/11,  
1046 4010–4026. <https://doi.org/10.1029/2019TC005806>
- 1047 Wunderlich, J. (2007). Mobile parametric sub-bottom profiler systems for shallow and medium depth  
1048 applications. *J. of the Acoustical Society of America* 122/5, 2983.
- 1049 Wunderlich J. and Müller S. (2003). High-resolution sub-bottom profiling using parametric  
1050 acoustics. *International Ocean Systems* 7/4, 6–11.
- 1051
- 1052

- 1053 **Supplement 1.** 3DPDF of the analyzed hypocenters recorded in period 1997 to 2018. in the investigated Bakar-Krk area  
1054 (data source: Croatian Earthquake Catalogue, CEC2018).
- 1055 **Supplement 2.** 3DPDF of the selected and extracted hypocenters used for the modelled fault planes in the subsurface of  
1056 Kostrena and Jadranovo. KF-Kostrena faults (1 and 2). JFZ – Jadranovo fault zone.
- 1057 **Supplement Tables.** Original data on measured fault planes with all parameters required for kinematic analysis in the study  
1058 area.
- 1059